UCLA
UCLA Previously Published Works

Title

High molecular weight amyloid β1-42 oligomers induce neurotoxicity via plasma membrane damage

Permalink

Journal

The FASEB Journal, 33(8)

ISSN

0892-6638

Authors

Yasumoto, Taro
Takamura, Yusaku
Tsuji, Mayumi
et al.

Publication Date

2019-08-01

DOI

10.1096/fj.201900604r

Peer reviewed

High molecular weight amyloid β₁-₄₂ oligomers induce neurotoxicity *via* plasma membrane damage

Taro Yasumoto,*,† Yusaku Takamura,‡ Mayumi Tsuji,† Takahiro Watanabe-Nakayama,§ Keiko Imamura,¶,‖,# Haruhisa Inoue,¶,‖,# Shiro Nakamura,** Tomio Inoue,** Atsushi Kimura,*,† Satoshi Yano,* Hisao Nishijo,‡ Yuji Kiuchi,† David B. Teplow,†† and Kenjiro Ono*,1

*Division of Neurology, Department of Internal Medicine, †Department of Pharmacology, School of Medicine, and **Department of Oral Physiology, School of Dentistry, Showa University, Tokyo, Japan; ‡System Emotional Science, Graduate School of Medicine and Pharmaceutical Sciences, University of Toyama, Toyama, Japan; §World Premier International Research Center Initiative (WPI)-Nano Life Science Institute, Kanazawa University, Kakuma-machi, Kanazawa, Japan; ¶Center for iPS Cell Research and Application (CiRA), Kyoto University, Kyoto, Japan; ‖iPSC-based Drug Discovery and Development Team, Riken BioResource Research Center (BRC), Kyoto, Japan; #Medical-risk Avoidance based on iPS Cells Team, Riken Center for Advanced Intelligence Project (AIP), Kyoto, Japan; and ††Department of Neurology, David Geffen School of Medicine at the University of California–Los Angeles (UCLA), Los Angeles, California, USA

ABSTRACT: Amyloid β-protein (Aβ) molecules tend to aggregate and subsequently form low MW (LMW) oligomers, high MW (HMW) aggregates such as protofibrils, and ultimately fibrils. These Aβ species can generally form amyloid plaques implicated in the neurodegeneration of Alzheimer disease (AD), but therapies designed to reduce plaque load have not demonstrated clinical efficacy. Recent evidence implicates amyloid oligomers in AD neuropathology, but the precise mechanisms are uncertain. We examined the mechanisms of neuronal dysfunction from HMW-Aβ₁-₄₂ exposure by measuring membrane integrity, reactive oxygen species (ROS) generation, membrane lipid peroxidation, membrane fluidity, intracellular calcium regulation, passive membrane electrophysiological properties, and long-term potentiation (LTP). HMW-Aβ₁-₄₂ disturbed membrane integrity by inducing ROS generation and lipid peroxidation, resulting in decreased membrane fluidity, intracellular calcium dysregulation, depolarization, and impaired LTP. The damaging effects of HMW-Aβ₁-₄₂ were significantly greater than those of LMW-Aβ₁-₄₂. Therapeutic reduction of HMW-Aβ₁-₄₂ may prevent AD progression by ameliorating direct neuronal membrane damage.—Yasumoto, T., Takamura, Y., Tsuji, M., Watanabe-Nakayama, T., Imamura, K., Inoue, H., Nakamura, S., Inoue, T., Kimura, A., Yano, S., Nishijo, H., Kiuchi, Y., Teplow, D. B., Ono, K. High molecular weight amyloid β₁-₄₂ oligomers induce neurotoxicity *via* plasma membrane damage. FASEB J. 33, 000–000 (2019). www.fasebj.org

KEY WORDS: Alzheimer disease · amyloid β-protein · membrane disruption

Neurodegenerative diseases [*e.g.*, Alzheimer disease (AD), Parkinson disease, and spinocerebellar ataxia] have

characteristic abnormal protein aggregates in the brain. In AD, amyloid plaques formed of amyloid β-protein (Aβ) and neurofibrillary tangles (NFTs) formed of hyperphosphorylated tau protein are the 2 cardinal neuropathological characteristics of the postmortem AD brain (1).

Human genetic association studies, biochemical analyses of AD plaque content, and various animal models with altered Aβ or tau expression strongly implicate Aβ and tau in AD pathogenesis (1). Furthermore, many *in vivo* and *in vitro* studies have demonstrated the neurotoxicity of amyloidogenic proteins. This neurotoxicity depends strongly on Aβ primary structure and aggregation state. For example, 2 predominant Aβ forms are produced in humans, comprising 40 (Aβ₁-₄₀) or 42 (Aβ₁-₄₂) amino acid residues, but the relative proportion of Aβ₁-₄₂ is particularly crucial for AD progression because this longer form is more prone to undergo aggregation and is inherently more toxic than Aβ₁-₄₀ (2). Aβ molecules form low MW (LMW) oligomers and high MW (HMW) oligomers such

as protofibrils (PFs) and finally form mature fibrils suggested to be the primary cause of neuronal dysfunction in AD (3). Although these Aβ aggregates can possibly directly cause neuronal injury by acting on synapses or indirectly cause it by activating astrocytes and microglia (2), evidence also supports the hypothesis that intermediate aggregates of Aβ, such as oligomers, play an important role in AD pathogenesis (1, 3–6). For instance, intracerebral injection of Aβ oligomers inhibits hippocampal long-term potentiation (LTP) in mice and rats (5, 7). Pyroglutamate-modified Aβ$_{1-42}$, which is enriched in AD brains compared with healthy controls, has been observed to aggregate faster than Aβ$_{1-42}$ by rapid formation of Aβ$_{1-42}$ oligomers, resulting in enhancement of neurotoxicity of Aβ$_{1-42}$ (8, 9). In addition, PFs are toxic to cultured neuronal cell lines and to primary neurons, and they cause profound changes in the electrical activity of mixed neuron-glia cultures (4). A form of familial AD has also been described that is due to a mutation in the gene that encodes the amyloid precursor protein resulting in the production of an Aβ species, [Glu22Gly]Aβ, with high propensity to form PFs (10).

Therefore, the canonical amyloid cascade hypothesis, positing that Aβ deposition leads to the formation of amyloid (senile) plaques and subsequently to NFTs and neuronal death, has been largely supplanted by the oligomer cascade hypothesis in which soluble oligomers are directly neurotoxic. However, the precise mechanisms of oligomer-mediated cytotoxicity remain incompletely understood, although evidence does suggest that the neuronal cell membrane is the chief site of oligomer-mediated neuronal damage. Membrane environment can enhance conformational change of Aβ to toxic β–sheet structure, which serves as nucleation sites for faster self-aggregation depending on lipid content within the membrane (11). In addition, ganglioside-containing membranes have been found to alter the aggregation pathways of Aβ; that is, low Aβ:ganglioside ratios yield an α-helical Aβ structure, whereas an increasing Aβ:ganglioside ratio promotes fibrillization (12). On the other hand, oligomers trigger a toxic cascade that involves the formation of ion-permeable membrane pores (13), interference with membrane receptor activities (14), and oxidation of membrane lipids (15). Membrane integrity is essential for maintaining cellular metabolism and intracellular calcium ion homeostasis, and dysregulation of these processes by Aβ triggers neuronal apoptosis (16, 17). Aβ can insert directly into the membrane and form a pore (18). Recently, using explicit solvent molecular dynamics simulations (19), Aβ oligomers have been reported to insert irreversibly into a membrane, followed by spontaneously forming ion channels, resulting in cell death. This result is consistent with the result that Aβ$_{1-42}$ can assemble into a β-barrel pore in lipid bilayers under optimized detergent micelle conditions (20). Although most of these studies used artificial membrane models, it was recently reported that small Aβ oligomers have higher membrane affinity than monomers in human embryonic kidney 293T (HEK293T) cells (21).

A clearer understanding of Aβ-membrane interactions is needed for future AD treatment development, especially because disease-modifying therapies that disassemble or remove amyloids have failed in clinical trials. In the present study, we examined the relationship between cellular membrane damage caused by HMW-Aβ oligomers and neurotoxicity using systematic *in vitro*, cellular, and synaptic assays, including measures of membrane integrity, reactive oxygen species (ROS) generation, lipid peroxidation, membrane fluidity, intracellular calcium concentration, membrane potentials, and LTP.

MATERIALS AND METHODS

Drugs and reagents

Highly purified human Aβ$_{1-42}$ was purchased from Peptide Institute (Osaka, Japan), and DMEM, Ham's F-12 medium, and all-*trans*-retinoic acid were procured from Wako Pure Chemicals (Osaka, Japan). Further, fetal bovine serum, 4-(2-hydroxyethyl)-1-piperazineethanesulfonic acid (HEPES), and EGTA were purchased from MilliporeSigma (Burlington, MA, USA). Penicillin G sodium, streptomycin sulfate, and amphotericin B were obtained from Thermo Fisher Scientific (Waltham, MA, USA). The other chemicals used were of the purest grade commercially available. Water was double distilled and deionized by using Milli-Q system (MilliporeSigma).

Preparation of Aβ

We prepared aggregate-free solutions of Aβ using size exclusion chromatography (SEC) (22, 23). The nominal monomer fraction is known as LMW because it comprises monomers mainly and dimers partly in rapid equilibrium at experimental peptide concentrations (22–24). To prepare LMW-Aβ$_{1-42}$ and HMW-Aβ$_{1-42}$, Aβ$_{1-42}$ was dissolved in DMSO at 2 mg/ml, sonicated for 3 min, and centrifuged for 20 min at 16,000 g. Next, the supernatant was fractionated using 10 mM phosphate buffer (pH 7.4) at a flow rate of 0.5 ml/min on a Superdex 75 HR column (GE Healthcare, Waukesha, WI, USA). The HMW peak eluted at 16–17 min (immediately after the column void volume) and was followed by the LMW peak at 26–27 min (**Fig. 1***A*). The central 60 s of the HMW and LMW peaks were individually collected and maintained at −80°C. In each preparation, the peptide concentration was determined using the Bradford-based Bio-Rad Protein Assay Dye Reagent Concentrate (Bio-Rad, Hercules, CA, USA). Aggregate concentration referred to monomeric Aβ$_{1-42}$ concentration. Typically, the concentrations of LMW-Aβ$_{1-42}$ and HMW-Aβ$_{1-42}$ were 17 and 12 μM, respectively.

Transmission electron microscopy

A 10-μl aliquot from each Aβ$_{1-42}$ fraction was dotted onto a glow-discharged, carbon-coated formvar grid (Okenshoji, Tokyo, Japan) and then incubated for 20 min. Then, the droplet was displaced with 2.5% (vol/vol) glutaraldehyde in water at an equal volume and incubated for 5 min. Lastly, 8 μl of 1% (vol/vol) uranyl acetate in water (Wako Pure Chemicals) was used to stain the peptide. The residual liquid was wicked off; the grid then was air dried, and the samples were observed using a JEM-1210 transmission electron microscope (TEM; Jeol, Tokyo, Japan).

Atomic force microscopy

We performed tapping mode high-speed atomic force microscopy (HS-AFM) (25, 26) at room temperature in liquid using a small cantilever (BL-AC10-DS; Olympus, Tokyo, Japan) with
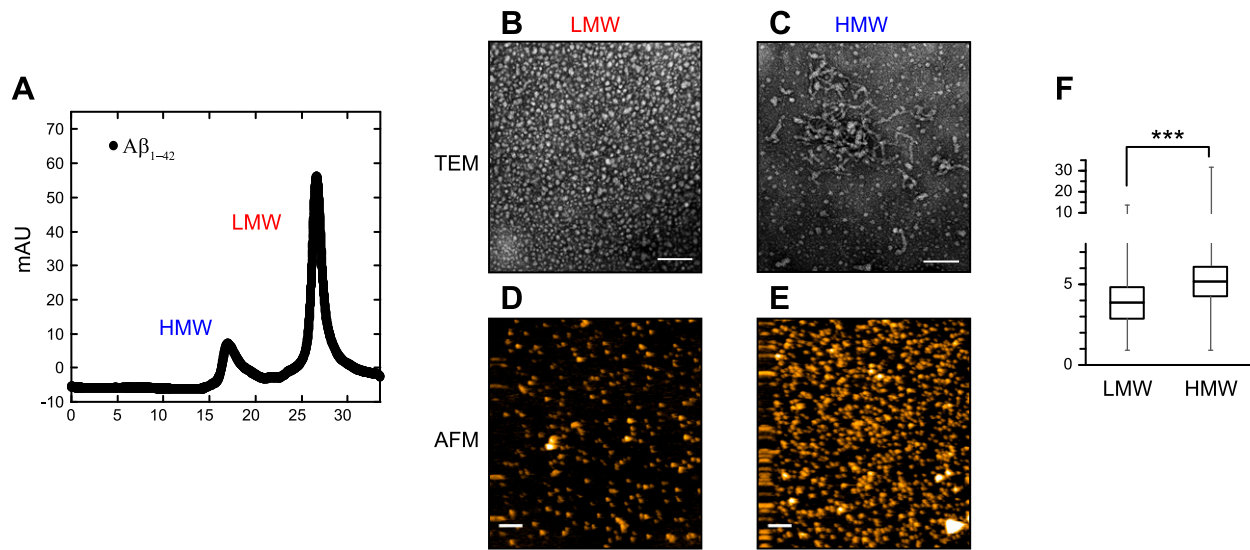
Figure 1. Preparation of HMW and LMW-Aβ$_{1-42}$ fraction. *A*) SEC of Aβ$_{1-42}$. The synthesized Aβ$_{1-42}$ was applied on a gel filtration column. The HMW peak was eluted at 16–17 min followed by the LMW peak at 26–27 min. *B–E*) TEM (*B, C*) and AFM (*D, E*) images of LMW-Aβ$_{1-42}$ (*B, D*) and HMW-Aβ$_{1-42}$ (*C, E*). Scale bars, 100 nm (*B, C*) and 100 nm (*D, E*). *Z* scale, 10 nm (*D, E*). *F*) Box plots of LMW-Aβ$_{1-42}$ and HMW-Aβ$_{1-42}$ aggregate sizes from AFM images (*D, E*). The boxes extend from the 25th to 75th percentile. The median values shown by the single bars in the boxes correspond to 3.9 nm for LMW-Aβ$_{1-42}$ and 5.2 nm for HMW-Aβ$_{1-42}$. The whiskers extend from the minimum to the 25th percentile and from the 75th percentile to the maximum. The asterisk indicates the statistically significant difference between LMW and HMW fractions. ***$P < 0.001$, *U* test.

resonance frequency *f* of 400–500 kHz and a spring constant *k* of 0.1 N/m. Further, an amorphous carbon tip was grown on each cantilever by electron beam deposition with a field emission scanning electron microscope (ERA8000-FE; STS-Elionix, North Billerica, MA, USA). Although the free oscillation amplitude was set at 1.5 nm, the set-point amplitude was 80–90% of the free amplitude. Next, LMW-Aβ$_{1-42}$ or HMW-Aβ$_{1-42}$ solution was introduced into a sample chamber, and the HS-AFM image sequences were processed using ImageJ software [*imagej.nih.gov/ij/*; National Institutes of Health (NIH), Bethesda, MA, USA] (27).

SH-SY5Y cell culture

SH-SY5Y (EC-94030304), a human neuroblastoma cell line, was acquired from the European Collection of Authenticated Cell Cultures (London, United Kingdom). The cells were cultured in DMEM and Ham's F-12 medium that contained 10% fetal bovine serum and antibiotic-antimycotic solution, and they were maintained under a humidified atmosphere of 5% CO$_2$ and 95% air at 37°C. SH-SY5Y cells are similar to neurons in terms of their morphologic and neurochemical properties, and they have been widely used to evaluate neuronal injury and death in response to neurotoxins and cerebral ischemia–reperfusion as *in vitro* disease models (28). To evaluate the effects of Aβ$_{1-42}$, SH-SY5Y cells were initially differentiated with all-trans retinoic acid. In the present study, differentiated SH-SY5Y cells were exposed to 5 μM of LMW-Aβ$_{1-42}$ or HMW-Aβ$_{1-42}$ for 30 min under sterile conditions.

Induced pluripotent stem cell culture

The healthy human induced pluripotent stem cell (iPSC) line 201B7 was maintained using the StemFit feeder-free culture system (Ajinomoto, Tokyo, Japan) (29). Cortical neurons were generated from iPSCs *via* transfection of Ngn2 using piggyBac vector with the tet-on system as previously reported in Imamura *et al.*

(30). Briefly, iPSCs were dissociated to single cells with Accumax solution (Innovative Cell Technologies, San Diego, CA, USA) and plated on Matrigel-coated 96-well plastic plates (BD Biosciences, San Jose, CA, USA) with a neural medium containing 1:1 DMEM/F12 (Thermo Fisher Scientific) and Neurobasal medium (Thermo Fisher Scientific) plus 1% N2 supplement, 2% B27 supplement, 10 ng/ml brain-derived neurotrophic factor (R&D Systems, Minneapolis, MN, USA), 10 ng/ml glial cell-derived neurotrophic factor (R&D Systems), 10 ng/ml neurotrophin-3 (R&D Systems), and 1 μg/ml doxycycline (Takara, Kusatsu, Japan).

3-(4,5-Dimethylthiazoyl-2-yl)-2,5-diphenyltetrazolium bromide viable cell assay

Cell viability was measured using the Cell Proliferation Kit I (Roche, Basel, Switzerland). This assay is based on the formation of blue formazan from 3-(4,5-dimethylthiazoyl-2-yl)-2,5-diphenyltetrazolium bromide (MTT) by mitochondrial dehydrogenases, which are active only in live cells. We conducted a preliminary experiment in which SH-SY5Y cells were exposed to different Aβ$_{1-42}$ concentrations (1, 2.5, 5, and 10 μM), and we found that 5 μM was the most suitable concentration for inducing cytotoxicity (Supplemental Fig. S1). After exposure to LMW-Aβ$_{1-42}$ or HMW-Aβ$_{1-42}$ for 30 min, cells were treated with DMSO to dissolve the formazan and formation was measured at 540 nm using a microplate reader (Spectra Max i3; Molecular Devices, Sunnyvale, CA, USA).

Lactate dehydrogenase release assay

Lytic cell death was measured using the Cytotoxicity Detection Kit (Roche). This kit quantifies cytotoxicity/cytolysis based on the measurement of lactate dehydrogenase (LDH) activity released into the medium when cell membrane integrity is lost. After exposure to 5 μM of LMW-Aβ$_{1-42}$ or HMW-Aβ$_{1-42}$ for 30 min, LDH in the culture medium was measured according to

substrate conversion at 490 nm using a microplate reader (Spectra Max i3).

Calcein and ethidium homodimer-1 (live/dead) cell assay

Surviving and dying SH-SY5Y cells were also measured by calcein and ethidium homodimer-1 costaining. Briefly, cells cultured in 96-well plates were exposed to 5 µM of LMW-Aβ$_{1-42}$ or HMW-Aβ$_{1-42}$ for 30 min and then stained with calcein AM (1 µM) and ethidium homodimer-1 (2 µM) (Molecular Probes, Eugene, OR, USA). Although the amount of green fluorescent calcein hydrolyzed by intracellular esterase is proportional to the number of viable cells, ethidium homodimer-1 only enters cells with damaged membranes and binds to nucleic acids, thus producing a bright red nuclear fluorescence relative to the number of dead cells. Labeled cells were measured at an excitation wavelength of 495 nm and emission wavelengths of 530 and 645 nm using the Spectra Max i3 or observed under a fluorescence microscope (BZ-X800; Keyence, Osaka, Japan) to assess the viability status of individual cells.

Water soluble tetrazolium cell viability assay

iPSCs were plated on Matrigel-coated 96-well plates with neural medium and 1 µg/ml doxycycline, cultured for 10 d, differentiated to cortical neurons as previously described, and then treated with 10 µM of LMW-Aβ$_{1-42}$ or HMW-Aβ$_{1-42}$ for 60 min. Cell viability was assessed using the water soluble tetrazolium (WST) assay using Cell Count Reagent (Nacalai, San Diego, CA, USA) according to the manufacturer's protocol.

Detection of ROS

SH-SY5Y cells were seeded on 96-well plates at a concentration of 1×10^5 cells/ml, loaded with the ROS-sensitive dye chloromethyl derivative of 2′,7′-dichlorodihydrofluorescein diacetate (CM-H$_2$DCFDA; Thermo Fisher Scientific) and treated with 5 µM of LMW-Aβ$_{1-42}$ or HMW-Aβ$_{1-42}$ for 30 min. A Spectra Max i3 was used to measure the fluorescence intensity at excitation and emission wavelengths of 488 and 525 nm, respectively. ROS accumulation is accompanied by an increase in 525 nm (green) fluorescence intensity.

Diphenyl-1-pyrenylphosphine lipid peroxidation assay

To detect phospholipid peroxidation in cell membranes, SH-SY5Y cells were stained with the probe diphenyl-1-pyrenylphosphine (DPPP; 5 µM) for 10 min at 37°C (Thermo Fisher Scientific) before Aβ treatment. DPPP is recognized to react with hydroperoxides to yield fluorescent phosphine oxide (DPPP = NO), but it is nonfluorescent until oxidized (31). After incubation with DPPP, cells were exposed with each Aβ species (5 µM) for 30 min and observed under a fluorescence microscope (BZ-X800; Keyence). Peroxidation is indicated by an increase in blue fluorescence emission.

Membrane fluidity

Membrane fluidity of SH-SY5Y cells was measured using the lipophilic pyrene probe pyrenedecanoic acid (PDA) in the Membrane Fluidity Kit (Marker Gene Technologies, Eugene, OR, USA) according to the manufacturer's protocol. In brief, 1×10^6 cells were exposed to 5 µM of LMW-Aβ$_{1-42}$ or HMW-Aβ$_{1-42}$ and stained at room temperature with the fluorescent lipid reagent containing PDA, which exists as either a monomer with peak emission at 400 nm from 360 nm excitation or as an excimer with peak emission near 470 nm from 360 nm excitation in response to spatial interaction in more fluid membranes. The ratio of fluorescence emission at 400 and 470 nm from 360 nm excitation (ratio of monomer to excimer) thus serves as an estimate of membrane fluidity. Ratio images in the membrane fluidity were calculated by monitoring the ratio of the fluorescence signals of PDA using confocal laser microscope Fluoview FV10i (Olympus). Briefly, the ratio image of the fluorescence at the emission wavelength of excimer to monomer was calculated pixel by pixel and displayed in grayscale.

Intracellular calcium concentration measurement

Intracellular ionized calcium concentration ([Ca^{2+}]$_i$) was measured using the FLIPR Calcium 5 Assay Kit (Molecular Devices). Briefly, we loaded SH-SY5Y cells with the FLIPR reagent diluted in HBSS with 20 mM HEPES (pH 7.4) for 60 min at 37°C. Cells were then exposed to either LMW-Aβ$_{1-42}$ or HMW-Aβ$_{1-42}$ (5 µM) in the presence or absence of extracellular calcium (0 mM Ca^{2+} HBSS with HEPES +0.3 mM EGTA). Further, after pretreatment with L-type calcium channel antagonist 10 µM nicardipine or 10 µM nicardipine plus N-methyl D-aspartate (NMDA) receptor antagonist 1 µM memantine, SH-SY5Y cells were exposed with either LMW-Aβ$_{1-42}$ or HMW-Aβ$_{1-42}$ (5 µM). In other experiments, cells were incubated with either LMW-Aβ$_{1-42}$ or HMW-Aβ$_{1-42}$ (5 µM) for 30 min and then exposed to 80 mM KCl. Changes in [Ca^{2+}]$_i$ were measured by observing FLIPR fluorescence signals at excitation and emission wavelengths of 485 and 525 nm, respectively, using Meta Xpress Image Acquisition (Molecular Devices).

Whole-cell patch-clamp recording

SH-SY5Y cells were grown in glass-bottom dishes that were coated with poly-D-lysine (MatTek, Ashland, MA, USA) and used for experiments until they were 50–70% confluence. SH-SY5Y cells were exposed to Aβ (5 µM) for 30 min as indicated. Patch electrodes (resistance 2.5–5.0 MΩ) were made from single-filament 1.5-mm outer diameter borosilicate capillary tubing (GD-1.5; Narishige, Amityville, NY, USA) using a microelectrode puller (P-97; Sutter Instrument, Novato, CA, USA). Electrodes were filled with an internal solution of the following composition (mM) for current-clamp experiments: 130 K-gluconate, 10 KCl, 10 HEPES, 0.4 EGTA, 2 MgCl$_2$, 2 Mg-ATP, and 0.3 Na$_2$-GTP (pH 7.25, 285–300 mOsm). The external solution contained (mM) 120 NaCl, 4 KCl, 1 CaCl$_2$, 0.3 MgCl$_2$, 0.4 MgSO$_4$, 0.5 NaH$_2$PO$_4$, 0.5 Na$_2$HPO$_4$, 29 NaHCO$_3$, and 17.5 glucose. All experiments were conducted at room temperature. Membrane potentials were recorded in current-clamp configuration with the Multiclamp 700B amplifier (Molecular Devices). The data were low-pass filtered at 10 kHz, sampled at 20 kHz (Digidata 1440; Molecular Devices) and then analyzed on a personal computer using pCLAMP 10.7 (Molecular Devices), Origin 2016 (Origin-Lab, Northampton, MA, USA), and Microsoft Excel (Microsoft, Redmond, WA, USA). Resting membrane potentials were immediately registered after forming the whole-cell configuration. Further, the liquid junction potential between bath solutions (12 mV) and pipette filling was subtracted from the membrane potential values. Input resistance was measured from the recordings of the voltage response to hyperpolarizing currents (300 ms in 10 pA steps). The membrane time constant (τ) was determined by fitting a single-exponential function to the charging transient of the same recording. Further, membrane capacitance was calculated by dividing the time constant by input resistance.

Electrophysiological recording from the mice hippocampus

Male C57BL/6 mice (5–7 wk old) were procured from Japan SLC (Shizuoka, Japan) and contained in an air-conditioned room in cages equipped with laboratory bedding under a 12 h/12 h light-dark cycle. Mice had free access to water and were fed a commercial diet (MF; Oriental Yeast, Tokyo, Japan). The experiments were conducted according to the *Guide for Care and Use of Laboratory Animals* at Toyama University and the *Guide for the Care and Use of Laboratory Animals* from the NIH.

Brains of the mice were rapidly removed, and several slices (300 μm thickness) comprising the transverse ventral hippocampal region were cut in ice-cold artificial cerebrospinal fluid (ACSF) containing (mM) 109 NaCl, 2 KCl, 1.25 $MgSO_4$, 1.25 NaH_2PO_4, 2 $CaCl_2$, 35 $NaHCO_3$, 20 HEPES, and 25 D-glucose) using vibratome (LiniarSlicer PRO7; Dosaka EM, Kyoto, Japan). The slices were incubated at 32°C in ACSF for at least 120 min with constant 95% oxygen/5% carbon dioxide aeration. Subsequently, the slice was transferred to a recording chamber and circulated with 3 ml of ACSF containing BSA (0.3 mg/ml) at 2 ml/min. Saline temperature was maintained at 34°C and continuously aerated using a gas exchange membrane module (Nagasep; Nagayanagi, Tokyo, Japan). During recording, the 3 ml of circulating ACSF was equilibrated using a dialysis tube (cutoff MW: 1000; Nippon Genetics, Düren, Germany) against 100 ml ACSF.

After a 15 min incubation period in the recording chamber, we recorded field excitatory postsynaptic potentials (fEPSPs). A bipolar stimulating electrode (manufactured from 2 urethane-insulated 50 μm stainless steel wires stripped of insulation over the distal 200 μm) was positioned on the Schaffer-collateral/commissural bundle in the CA3 hippocampal subfield; a recording glass micropipette (2–6 MΩ, packed with 3 mM NaCl) was positioned on the CA1 stratum radiatum. The Schaffer-collateral/commissural bundle was stimulated with 50 μs monophasic square pulses at 20 s intervals. Stimulus intensity was adjusted between 60 and 200 μA to yield 40% of the maximal fEPSP amplitude (baseline stimulation). LTP was induced by 20 s apart of 2 high-frequency stimulation (HFS; 100 pulses at 100 Hz) trains by the same monophasic square pulses. The evoked potentials were amplified (×1000), filtered (0.1–1000 Hz), digitized (24 kHz), and stored on a computer for offline analysis with the PowerLab system (AD Instruments, Sydney, New South Wales, Australia). Herein, LTP values are presented as the percentage of the average fEPSP slope (80% of peak to bottom) relative to the mean baseline value before HFS. In all groups, all hippocampal slices were derived from different animals. Slices were exposed to LMW-Aβ$_{1–42}$ or HMW-Aβ$_{1–42}$ for 1 h before HFS.

Statistical analysis

Each measurement was repeated 3 times. The mean heights derived from atomic force microscopy (AFM) imaging were compared between LMW-Aβ$_{1–42}$ and HMW-Aβ$_{1–42}$ groups using the Mann-Whitney U test. Results of all cellular experiments are expressed as the means ± SEM. The effects of various treatments were compared to untreated SH-SY5Y cells by 1-way ANOVA followed by Dunnett *post hoc* test or unpaired Student's *t* test for pair-wise comparisons. Results of iPSC assays were analyzed using ANOVA followed by Tukey *post hoc* test using SPSS software (IBM SPSS, Chicago, IL, USA). Results of synaptic transmission and LTP experiments were analyzed by ANOVA followed by Tukey-Kramer *post hoc* test using R v.3.4.3 (R Foundation for Statistical Computing, Vienna, Austria). A value of $P < 0.05$ was considered statistically significant for all tests.

RESULTS

TEM and atomic force microscopy imaging

First, the assembly properties of Aβ$_{1–42}$ preparations were determined using TEM and HS-AFM. The assemblies within the LMW and HMW SEC fractions had morphologies consistent with those previously reported (Fig. 1*B*, *C*) (22, 23, 32). The LMW-Aβ$_{1–42}$ fraction consisted of irregular, globular structures of mean diameter 3.78 ± 0.51 nm ($n = 20$) that sometimes had threadlike components (Fig. 1*B*) (6, 33), whereas the HMW-Aβ$_{1–42}$ fraction consisted of some short, relatively narrow (5 nm) structures that resembled beaded chains, consistent with PF morphology (Fig. 1*C*) (23, 32). AFM images also revealed structural differences between LMW and HMW. Although both fractions contained globule structures (Fig. 1*D*, *E*), these differed significantly in size, producing aggregates of distinct individual height (Fig. 1*F*). The LMW-Aβ$_{1–42}$ was significantly smaller than the HMW-Aβ$_{1–42}$ (Fig. 1*F*).

HMW-Aβ$_{1-42}$ is more cytotoxic than LMW-Aβ$_{1-42}$ to SH-SY5Y neuroblastoma cells

There were also substantial differences in terms of the cytotoxicity of these fractions. Exposure to each Aβ$_{1-42}$ fraction (5 μM, 30 min) caused in a significant decrease in viable SH-SY5Y cell number compared with untreated controls as evidenced by blue formazan from MTT viable cell assay (LMW-Aβ$_{1-42}$: 86.1% of control, HMW-Aβ$_{1-42}$: 75.8% of control, ANOVA, $P < 0.01$), but the reduction was significantly greater following HMW-Aβ$_{1-42}$ exposure ($P < 0.05$; **Fig. 2A**).

Neurotoxicity of each Aβ$_{1-42}$ fraction was further evaluated by analyzing LDH activity released from dead cells (Fig. 2*B*). Again, both fractions induced significant cell death compared to untreated controls (control: 18.9%, LMW-Aβ$_{1-42}$: 30.0%, HMW-Aβ$_{1-42}$: 37.5%, ANOVA, $P < 0.01$), but HMW-Aβ$_{1-42}$ induced significantly greater LDH release than LMW-Aβ$_{1-42}$ ($P < 0.05$), indicating greater cytotoxicity.

To directly examine Aβ cytotoxicity at the individual cell level, SH-SY5Y cells were stained with calcein AM and ethidium homodimer-1 (Fig. 2*C*). Calcein AM is enzymatically converted to green fluorescent calcein in the cytoplasm by esterases of live cells, whereas only cells with damaged membranes are permeable to red fluorescence ethidium homodimer-1. Consistent with MTT and LDH assay results, both Aβ fractions increased the ethidium homodimer-1 (dead/dying cell) to calcein (live cell) ratio (control: 7.37%, LMW-Aβ$_{1-42}$: 16.43%, HMW-Aβ$_{1-42}$: 21.33%, $P < 0.01$), but the damage was significantly greater following HMW-Aβ$_{1-42}$ exposure than to LMW-Aβ$_{1-42}$ exposure ($P < 0.05$). Control cells remained morphologically intact as revealed by phase-contrast microscopy (Fig. 2*D*) and viable as evidenced by intense green fluorescence emission from the cytoplasm and unstained nuclei (Fig. 2*E*). LMW-Aβ$_{1-42}$ and HMW-Aβ$_{1-42}$ (5 μM for 30 min) altered cell morphology (Fig. 2*F*, *H*) and increased the number of cells with red fluorescent nuclei, but the number of red fluorescent nuclei was significantly higher in
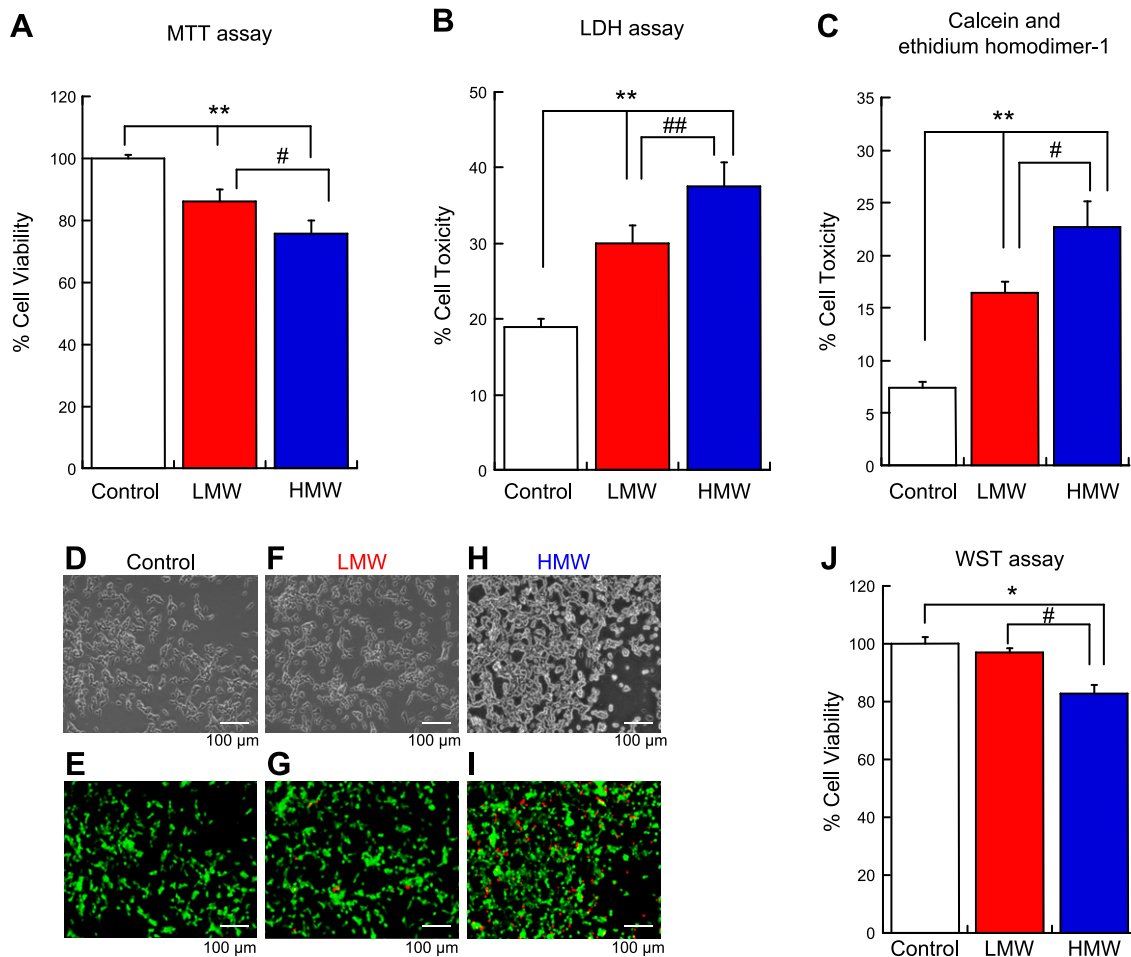
Figure 2. HMW-Aβ$_{1-42}$ is more cytotoxic than LMW-Aβ$_{1-42}$ to SH-SY5Y neuroblastoma cells (*A–I*) and iPSC-derived cortical neurons (*J*). *A*) MTT assay. Each value is expressed relative to the viability of untreated control cultures (set to 100%). The formazan optical density (OD) value of the control cells was 0.3223 ± 0.0098. Values are expressed as means + SEM of 12 independently treated culture wells. *B*) LDH assay. Values are expressed as means + SEM of 24–36 independently treated culture wells. *C*) Calcein AM and ethidium homodimer-1 assay. Values are expressed as means + SEM of 24 independently treated culture wells. *D–I*) SH-SY5Y cells that were observed under a phase-contrast microscope (*D, F, H*), and fluorescence images of calcein and ethidium homodimer-1 staining (*E, G, I*). Images (*D, E*): Untreated control SH-SY5Y cells. Images (*F, G*): SH-SY5Y cells exposed to 5 μM LMW-Aβ$_{1-42}$. Images (*H, I*): SH-SY5Y cells exposed to 5 μM HMW-Aβ$_{1-42}$. Scale bars, 100 μm. *J*) WST assay. Exposure to HMW-Aβ$_{1-42}$ decreased the viability of human iPSC-derived neurons. Values are expressed as means + SEM of 6 samples independently treated culture wells. *$P < 0.05$, **$P < 0.01$ *vs.* control cells. #$P < 0.05$, ##$P < 0.01$ *vs.* LMW-Aβ$_{1-42}$ group.

cultures treated with HMW-Aβ$_{1-42}$ than in those treated with LMW-Aβ$_{1-42}$ (**Fig. 2***G, I*).

Finally, the greater cytotoxicity of HMW-Aβ$_{1-42}$ was confirmed in iPSC-derived cortical neurons using the WST assay (**Fig. 2***J*). Exposure to HMW-Aβ$_{1-42}$ (10 μM for 60 min) resulted in a significantly greater decrease in WST than both control cells and cells exposed to the same dose of LMW-Aβ$_{1-42}$ (control: 100%, LMW-Aβ$_{1-42}$: 97.1%, HMW-Aβ$_{1-42}$: 82.7%, all $P < 0.05$).

HMW-Aβ$_{1-42}$ exposure induces more severe oxidative stress than LMW-Aβ$_{1-42}$ in SH-SY5Y cells

The ROS-sensitive dye CM-H$_2$DCFDA was used as an indicator of ROS formation to examine the effects of Aβ$_{1-42}$ exposure on hydrogen peroxide production (**Fig. 3***A–G*). As shown in Fig. 3*A*, ROS generation significantly increased in SH-SY5Y cells exposed to either Aβ$_{1-42}$ assembly (5 μM) for 30 min or untreated control cells (control: 18.011×10^5 FI/μg protein, LMW-Aβ$_{1-42}$: 36.39×10^5 FI/μg protein, HMW-Aβ$_{1-42}$: 53.54×10^5 FI/μg protein, $P < 0.01$). Consistent with cell cytotoxicity assays, HMW-Aβ$_{1-42}$ resulted in greater oxidative stress as evidenced by the more intense green CM-H$_2$DCFDA fluorescence than cells treated with an equivalent dose of LMW-Aβ$_{1-42}$ ($P < 0.05$). Examples of individual untreated CM-H$_2$DCFDA–stained cells, those treated with LMW-Aβ$_{1-42}$, or those treated with HMW-Aβ$_{1-42}$ are shown in Fig. 3*E–G*, respectively.

Enhanced membrane lipid peroxidation by HMW-Aβ$_{1-42}$

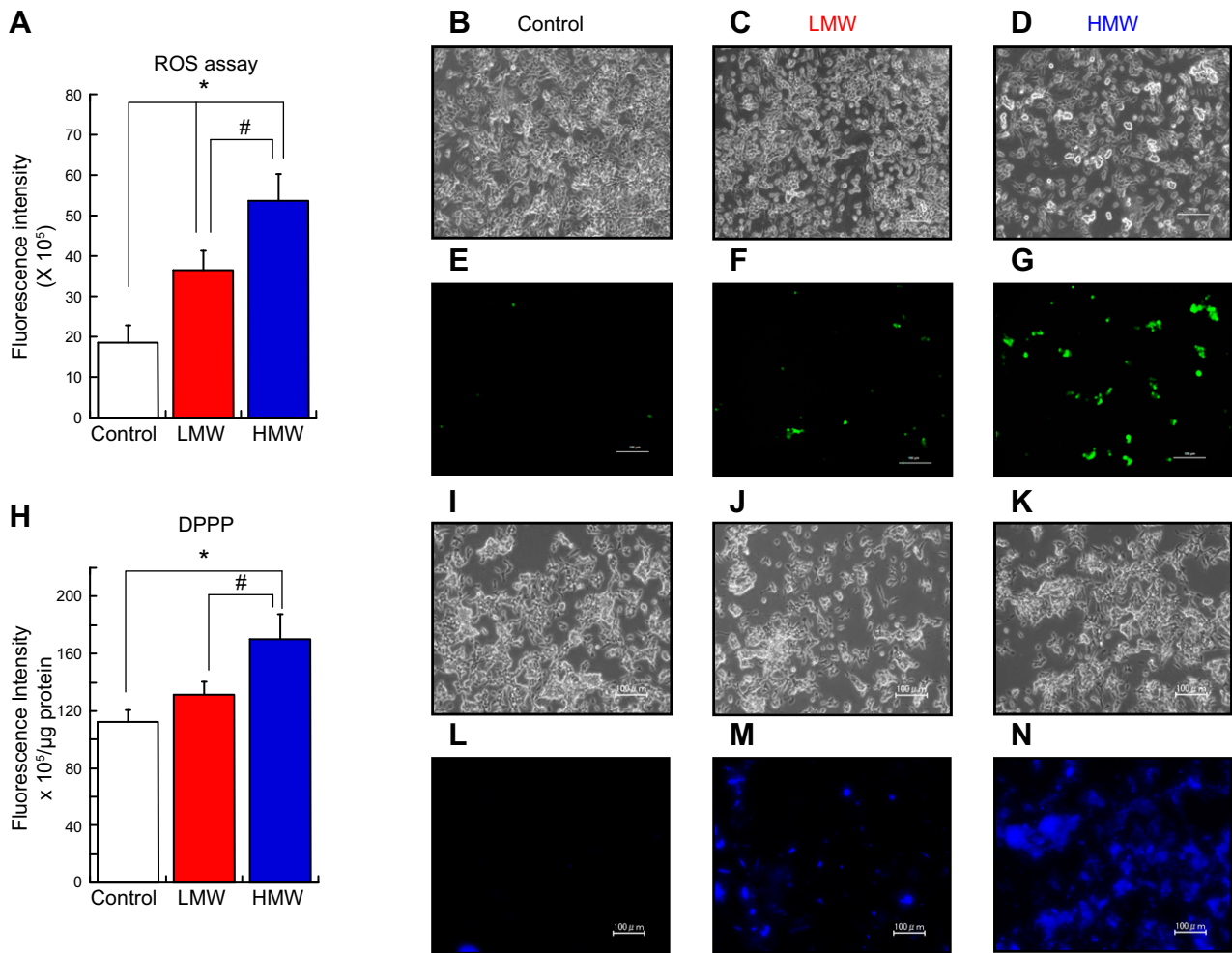Lipid peroxidation was measured by DPPP assay in SH-SY5Y cells after treatment with 5 μM LMW-Aβ$_{1-42}$ or

Figure 3. HMW-Aβ$_{1-42}$ induces more severe oxidative stress and membrane lipid peroxidation than LMW-Aβ$_{1-42}$ in SH-SY5Y cells. *A*) ROS generation. Each value represents the mean + SEM of 12 independently treated culture wells. *$P < 0.01$ *vs.* control cells. #$P < 0.05$ *vs.* LMW-Aβ$_{1-42}$ group. *B–G*) The SH-SY5Y cells observed using a phase-contrast microscope (*B–D*) and CM-H$_2$DCFDA fluorescence (*E–G*), untreated SH-SY5Y cells (*B, E*), SH-SY5Y cells exposed to 5 μM LMW-Aβ$_{1-42}$ (*C, F*), SH-SY5Y cells exposed to 5 μM HMW-Aβ$_{1-42}$ (*D, G*). Scale bars, 200 μm. *H*) DPPP assay. Each value represents the mean ± SEM of 12 independently treated culture wells. *$P < 0.01$ *vs.* control cells. #$P < 0.05$ *vs.* LMW-Aβ$_{1-42}$ group. *I–N*) The SH-SY5Y cells were observed under a phase-contrast microscope (*I–K*), DPPP fluorescence (*L–N*), untreated SH-SY5Y cells (*I, L*), SH-SY5Y cells exposed to 5 μM LMW-Aβ$_{1-42}$ (*J, M*). SH-SY5Y cells exposed to 5 μM HMW-Aβ$_{1-42}$ (*K, N*). Scale bars, 100 μm.

HMW-Aβ$_{1-42}$ (Fig. 3*H–N*). Again, both Aβ$_{1-42}$ fractions induced significant membrane phospholipid peroxidation compared with untreated control cells, but the severity of peroxidation as estimated by blue fluorescence intensity was greater following HMW-Aβ$_{1-42}$ treatment (control: 111.9 × 10^5 FI/μg protein, LMW-Aβ$_{1-42}$: 130.9 × 10^5 FI/μg protein, HMW-Aβ$_{1-42}$: 170.3 × 10^5 FI/μg protein, $P < 0.01$ *vs.* control, $P < 0.05$ *vs.* LMW-Aβ$_{1-42}$) (Fig. 3*H*). Fluorescence images of individual DPPP-stained cells during Aβ$_{1-42}$ exposure are presented in Fig. 3*L–N*.

HMW-Aβ$_{1-42}$ has greater effects on cell membrane fluidity than LMW-Aβ$_{1-42}$

Membrane phospholipid peroxidation is assumed to alter multiple membrane structural and function properties including barrier function, fluidity, and lipid raft properties. **Figure 4** shows that both HMW-Aβ$_{1-42}$ and LMW-Aβ$_{1-42}$ (5 μM, 30 min) significantly reduced

SH-SY5Y cell membrane fluidity compared with non-treated control cells (control: 100 ± 3.72%, LMW-Aβ$_{1-42}$: 83.3 ± 4.3%, HMW-Aβ$_{1-42}$: 70.7 ± 4.99%, $P < 0.01$ *vs.* control). Furthermore, HMW-Aβ$_{1-42}$ produced a larger decrease in fluidity than did LMW-Aβ$_{1-42}$ ($P < 0.05$). Consistent with the results of the cell membrane fluidity assay, HMW-Aβ$_{1-42}$ led to a decrease in membrane fluidity as evidenced by a darker black level of ratio image than untreated cells. Individual ratio images of cells treated untreated, treated with LMW-Aβ$_{1-42}$, or treated with HMW-Aβ$_{1-42}$ are shown in Fig. 4*C, E, G*, respectively.

Intracellular Ca^{2+} dysregulation following LMW-Aβ$_{1-42}$ and HMW-Aβ$_{1-42}$ exposure

We next investigated the effects of LMW-Aβ$_{1-42}$ and HMW-Aβ$_{1-42}$ on [Ca^{2+}]$_i$ homeostasis using Meta Xpress Image Acquisition (**Fig. 5**).

Exposure of SH-SY5Y cells to LMW- or HMW-Aβ$_{1-42}$ triggered an elevation in [Ca^{2+}]$_i$. This increase reached a peak in ~10 s after exposure and [Ca^{2+}]$_i$ remained elevated at a nearly constant plateau level thereafter (Fig. 5A). The peak increase did not differ significantly between LMW-Aβ$_{1-42}$ and HMW-Aβ$_{1-42}$ treatments, but the plateau level was higher in cells exposed to HMW-Aβ$_{1-42}$ (after 60 s of exposure, LMW-Aβ$_{1-42}$: 106.87 $\pm$ 1.38%, HMW-Aβ$_{1-42}$:

112.31 $\pm$ 1.84%, $P < 0.05$). To confirm that this [Ca^{2+}]$_i$ increase was because of influx, we also measured [Ca^{2+}]$_i$ in the absence of extracellular Ca^{2+}. Removal of extracellular Ca^{2+} completely inhibited the [Ca^{2+}]$_i$ increase evoked by 5 μM LMW- or HMW-Aβ$_{1-42}$ (Fig. 5A), indicating that Aβ$_{1-42}$ exposure induces extracellular Ca^{2+} influx.

To investigate whether this Ca^{2+} influx is mediated by L-type calcium channels, [Ca^{2+}]$_i$ changes in response to LMW- and HMW-Aβ$_{1-42}$ stimulation were also measured in the presence of the L-type voltage-dependent Ca^{2+} channel (VDCC) blocker nicardipine. Pretreatment with nicardipine (10 μM) caused significant decrease in the [Ca^{2+}]$_i$ elevation measured after 75 s of HMW-Aβ$_{1-42}$ (5 μM) exposure (HMW-Aβ$_{1-42}$: 110 $\pm$ 2.03%, nicardipine pretreatment: 105.4 $\pm$ 1.28%, $P < 0.05$ $vs.$ HMW-Aβ$_{1-42}$) (Fig. 5B). These findings suggest that HMW-Aβ$_{1-42}$ promotes calcium influx through L-type VDCCs in SH-SY5Y cells. Furthermore, in exposure to LMW-Aβ$_{1-42}$ or HMW-Aβ$_{1-42}$, pretreatment with nicardipine (10 μM) plus memantine (1 μM) resulted in a marked reduction of [Ca^{2+}]$_i$ compared to pretreatment with nicardipine alone (after 25 s of HMW-Aβ$_{1-42}$ exposure: nicardipine pretreatment: 117.3 $\pm$ 1.09%, nicardipine plus memantine pretreatment: 103.9 $\pm$ 0.94%, $P < 0.01$ $vs.$ pretreatment with nicardipine) (Fig. 5B). Memantine modulates the glutamatergic system, likely by blocking Ca^{2+} influx through NMDA receptors.

We next investigated the effects of LMW-Aβ$_{1-42}$ and HMW-Aβ$_{1-42}$ pre-exposure (5 μM for 30 min) on intracellular calcium homeostasis in SH-SY5Y cells. The exposure to 80 mM KCl, known to cause depolarization and Ca^{2+} entry via VDCCs, resulted in increased [Ca^{2+}]$_i$ in SH-SY5Y cells (Fig. 5C). However, KCl-induced [Ca^{2+}]$_i$ increases were significantly reduced by pre-exposure to LMW- or HMW-Aβ$_{1-42}$ compared with Aβ$_{1-42}$-untreated cells (after 19.5 s of exposure to 80 mM KCl alone: 144.42 $\pm$ 2.69%, plus LMW-Aβ$_{1-42}$: 112.83 $\pm$ 4.52%, $P < 0.05$ $vs.$ KCl, plus HMW-Aβ$_{1-42}$: 113.98 $\pm$ 9.90%, $P < 0.01$ $vs.$ KCl). This suppression of depolarization-evoked [Ca^{2+}]$_i$ elevation was greater in the presence of HMW-Aβ$_{1-42}$ than LMW-Aβ$_{1-42}$ (after 45.5 s of exposure, LMW-Aβ$_{1-42}$: 212.39 $\pm$ 6.39%, HMW-Aβ$_{1-42}$: 163.8 $\pm$ 14.8%, $P < 0.05$). Overall, these findings suggest that an exposure to Aβ$_{1-42}$ damages voltage-gated calcium channels, reduce their membrane insertion, or decrease voltage-gated activity due to changes in the membranes structure.
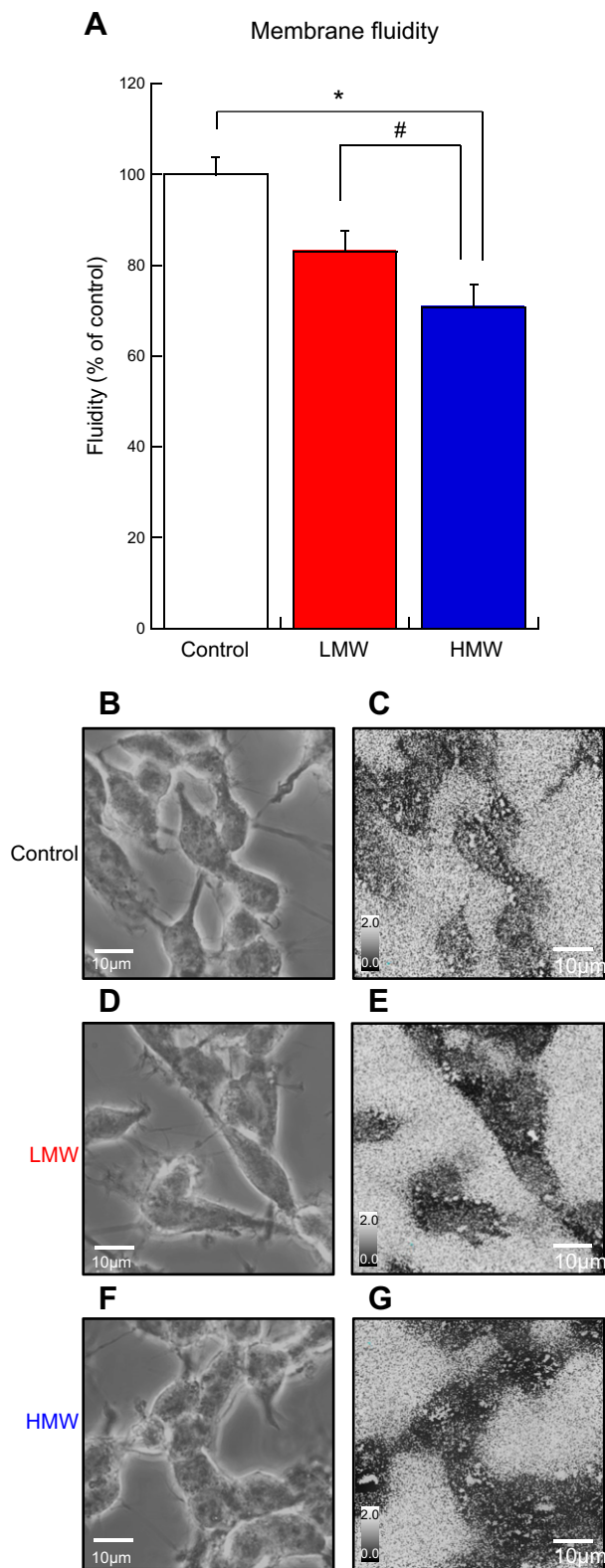

Figure 4. HMW-Aβ$_{1-42}$ reduces cell membrane fluidity to a greater extent than LMW-Aβ$_{1-42}$. Fluorescence emission was measured at both 400 and 470 nm from 360 nm excitation. *A*) Membrane fluidity of the control cells was 0.751 $\pm$ 0.086 (470 nm/400 nm ratio/μg protein). Each value is expressed relative to the control value (set as 100%). *$P < 0.01$ $vs.$ control cells, #$P < 0.05$ $vs.$ LMW-Aβ$_{1-42}$ group. *B–G*) The SH-SY5Y cells observed under a phase-contrast microscope are shown in *B, D,* and *F*. Ratio image of fluorescence is shown in *C, E,* and *G*. SH-SY5Y cells exposed to 5 μM LMW-Aβ$_{1-42}$ (*D, E*), SH-SY5Y cells exposed to 5 μM HMW-Aβ$_{1-42}$ (*F, G*). Scale bars, 10 μm.
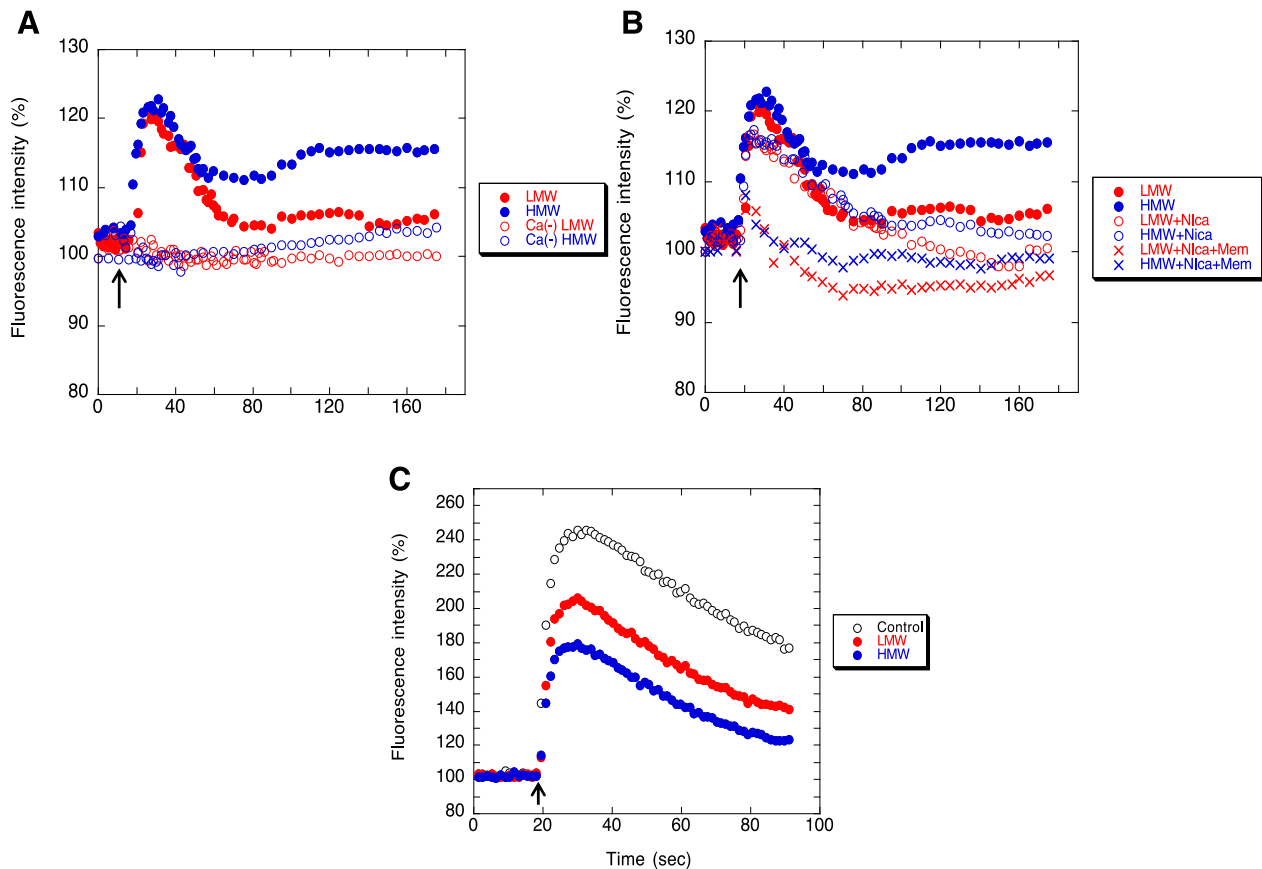
Figure 5. HMW-Aβ$_{1-42}$ more strongly inhibits depolarization-evoked Ca^{2+}-influx than LMW-Aβ$_{1-42}$. Effects of LMW-Aβ$_{1-42}$ and HMW-Aβ$_{1-42}$ on [Ca^{2+}]$_i$ in SH-SY5Y cells. *A*) Changes in [Ca^{2+}]$_i$ were measured fluorometrically in untreated SH-SY5Y cells and in cells exposed to 5 μM LMW-Aβ$_{1-42}$ or HMW-Aβ$_{1-42}$. Arrow indicates the addition of Aβ$_{1-42}$ to SH-SY5Y cells. Changes in [Ca^{2+}]$_i$ during exposure to 5 μM LMW-Aβ$_{1-42}$ or HMW-Aβ$_{1-42}$ were also examined in Ca^{2+}-free buffer. *B*) SH-SY5Y cells were pretreated with 10 μM nicardipine (Nica) or 10 μM Nica +1 μM memantine (Mem) for 5 min or left untreated, followed by exposure to LMW-Aβ$_{1-42}$ or HMW-Aβ$_{1-42}$. Arrows indicate the addition of Aβ$_{1-42}$ to the SH-SY5Y cells. Nica significantly reduced the Aβ$_{1-42}$-induced [Ca^{2+}]$_i$ increase (after 75 s; $P < 0.05$). Furthermore, alterations in [Ca^{2+}]$_i$ levels by exposure to LMW-Aβ$_{1-42}$ or HMW-Aβ$_{1-42}$ after pretreating the cells with Nica + Mem showed a significant decrease compared to Nica pretreatment (25–70 s; $P < 0.01$). *C*) Increases in [Ca^{2+}]$_i$ evoked by 80 mM KCl in SH-SY5Y cells exposed to 5 μM LMW-Aβ$_{1-42}$ or HMW-Aβ$_{1-42}$ for 30 min. Arrow indicates the addition of 80 mM KCl.

Sustained depolarization of the SH-SY5Y cell membrane potential following exposure to LMW-Aβ$_{1-42}$ or HMW-Aβ$_{1-42}$

In light of results showing disruption of membrane integrity, we examined the passive membrane electrophysiological properties (resting potential, input resistance, time constant, and whole-cell capacitance) of SH-SY5Y cells exposed to 5 μM LMW-Aβ$_{1-42}$ or HMW-Aβ$_{1-42}$ for 30 min. **Figure 6** shows representative traces in response to 400 ms hyperpolarizing and depolarizing current pulses in untreated cells and cells exposed to each Aβ assembly type. The resting potential was significantly elevated in SH-SY5Y cells exposed to HMW-Aβ$_{1-42}$ (5 μM) compared with untreated control cells and LMW-Aβ$_{1-42}$–exposed cells (control: −45.88 ± 0.92 mV, LMW-Aβ$_{1-42}$: −45.14 ± 0.88 mV, HMW-Aβ$_{1-42}$: −42.70 ± 0.67 mV, $P < 0.05$ *vs.* control, $P < 0.05$ *vs.* LMW-Aβ$_{1-42}$) (Fig. 6*D*). Furthermore, input resistance was significantly lower following HMW-Aβ$_{1-42}$ exposure (control: 3575.9 ± 213.59 MΩ, LMW-Aβ$_{1-42}$: 3404.2 ± 232.42 MΩ, HMW-Aβ$_{1-42}$: 2475.7 ± 191.16 MΩ,

$P < 0.05$ *vs.* control, $P < 0.05$ *vs.* LMW-Aβ$_{1-42}$; Fig. 6*E*). However, whole-cell capacitance did not significantly differ among treatment groups (control: 24.2 ± 1.22 pF, LMW-Aβ$_{1-42}$: 26.03 ± 1.39 pF, HMW-Aβ$_{1-42}$: 22.52 ± 1.67 pF; Fig. 6*F*). These data suggest that HMW-Aβ$_{1-42}$ induces greater passive membrane ion leakage than does LMW-Aβ$_{1-42}$, consistent with vital staining results.

HMW-Aβ$_{1-42}$ impairs hippocampal LTP

Finally, we examined the effects of LMW-Aβ$_{1-42}$ and HMW-Aβ$_{1-42}$ on basal synaptic transmission and HFS-induced LTP in the CA1 subfield of hippocampal slices (**Fig. 7**). In the Schaffer-collateral/commissural pathway, neither LMW-Aβ$_{1-42}$ nor HMW-Aβ$_{1-42}$ (1 μM for 60 min) altered the strength of electrically evoked basal synaptic transmission as measured by the ratio of fEPSP slope in treated slices compared with untreated control slices [control: 103 ± 4% ($n = 9$), LMW-Aβ$_{1-42}$: 100 ± 3% ($n = 6$), HMW-Aβ$_{1-42}$: 98 ± 4% ($n = 7$); $F_{2, 19} = 0.445$, $P = 0.647$; Fig. 7*A, B*].
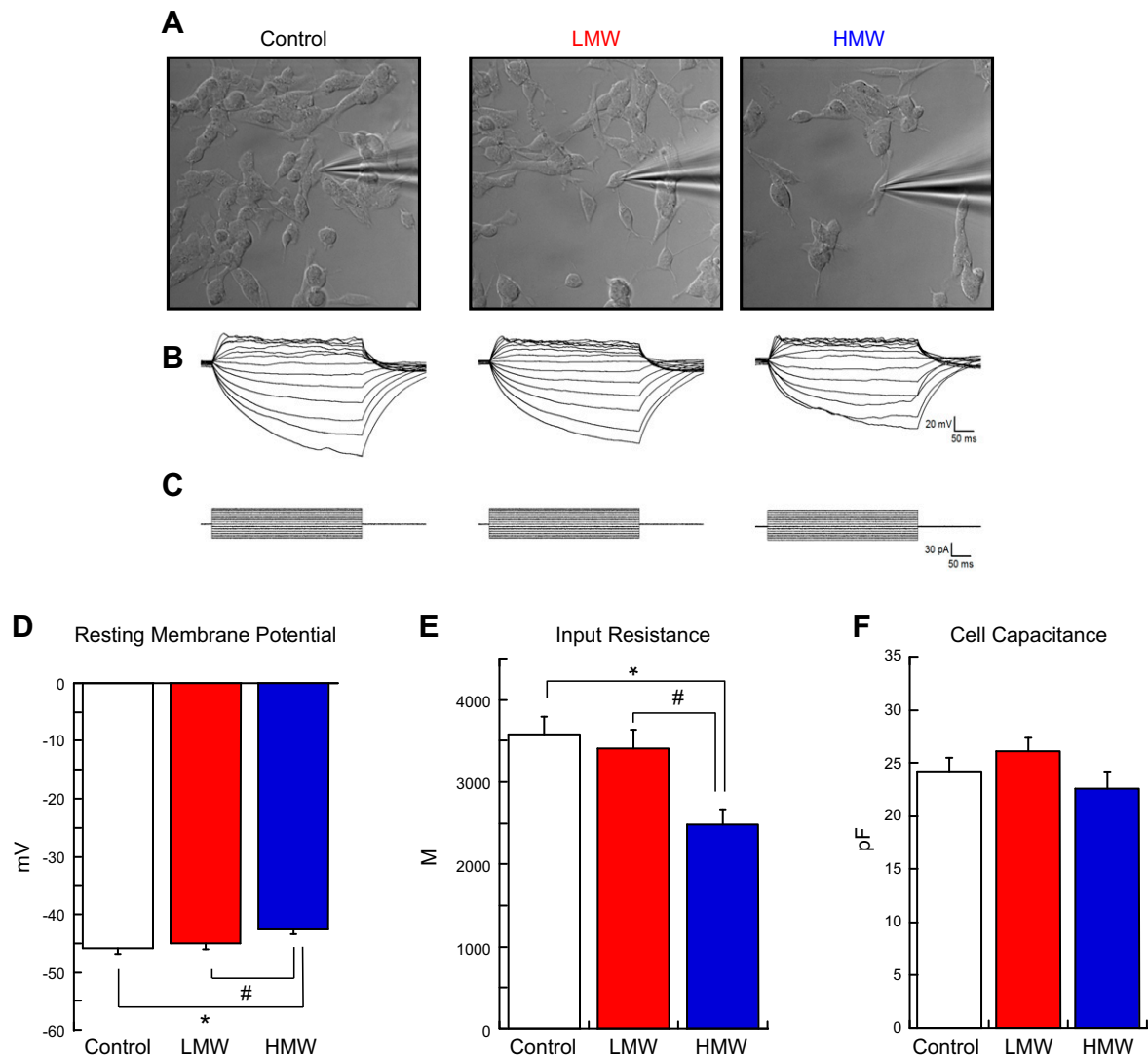
Figure 6. HMW-Aβ$_{1-42}$ elevates membrane potential and input resistance to a greater extent than LMW-Aβ$_{1-42}$. *A*) Translucent images of untreated control (left), LMW-Aβ$_{1-42}$–exposed (middle), and HMW-Aβ$_{1-42}$–exposed SH-SY5Y cells (right). *B, C*) Representative voltage responses (*B*) to 400 ms hyperpolarizing and depolarizing current pulses (*C*) from untreated control cells (left), LMW-Aβ$_{1-42}$–exposed cells (middle), and HMW-Aβ$_{1-42}$–exposed cells (right). *D–F*) Average resting membrane potential (*D*), input resistance (*E*), and whole-cell capacitance (*F*) measured in untreated controls (white bars), LMW-Aβ$_{1-42}$–exposed cells (red bars), and HMW-Aβ$_{1-42}$–exposed cells (blue bars). *$P < 0.05$ *vs.* controls, #$P < 0.05$ *vs.* LMW-Aβ$_{1-42}$ group.

We next tested the effects of each Aβ$_{1-42}$ assembly on hippocampal LTP (Fig. 7*A, C*). At 50–60 min after HFS, the ratio of the fEPSP slope relative to the control group was not significantly reduced by LMW-Aβ$_{1-42}$ but was significantly lower in slices treated with HMW-Aβ$_{1-42}$ [control: $176 \pm 9\%$ (*n* = 12 slices from 12 mice), LMW-Aβ$_{1-42}$: $166 \pm 14\%$ (*n* = 7 slices from 7 mice), HMW-Aβ$_{1-42}$: $138 \pm 10\%$ (*n* = 8 slices from 8 mice); F$_{2, 23}$ = 3.86, $P = 0.036$; Fig. 7*A, C*]. Thus, HMW-Aβ$_{1-42}$, but not LMW-Aβ$_{1-42}$, significantly reduced LTP formation ($P < 0.05$).

DISCUSSION

Although recent evidence suggested that low-order oligomers such as dimers, trimers, and HMW oligomers such as PFs exhibit cellular and synaptic toxicities (1, 3–6), the pathogenic mechanisms for Aβ-induced cell dysfunction and death in AD remain controversial, at least in part, because the relative toxicities of various Aβ conformations are unclear. Nonetheless, numerous studies have demonstrated the disruption of organelle and cellular homeostasis by Aβ aggregates, which in turn can trigger or exacerbate excitotoxicity, oxidative stress, calcium dysregulation, and a shift in the balance between pro- and antiapoptotic factors (34). Actually, assemblies including Aβ-derived diffusible ligands, HMW oligomers, and low-order oligomers are found in cerebrospinal fluid (35), plasma (36), and interstitial fluid (37) of patients with AD, but it is unclear how brain cells exposed to Aβ oligomers become dysfunctional and deteriorate. One unifying explanation is the potential effect of Aβ oligomers on membranes that affects plasma membrane permeation and causes mitochondrial dysfunction and lysosomal leakage, resulting in effects such as loss of ionic gradients, plasma membrane potential, and mitochondrial membrane
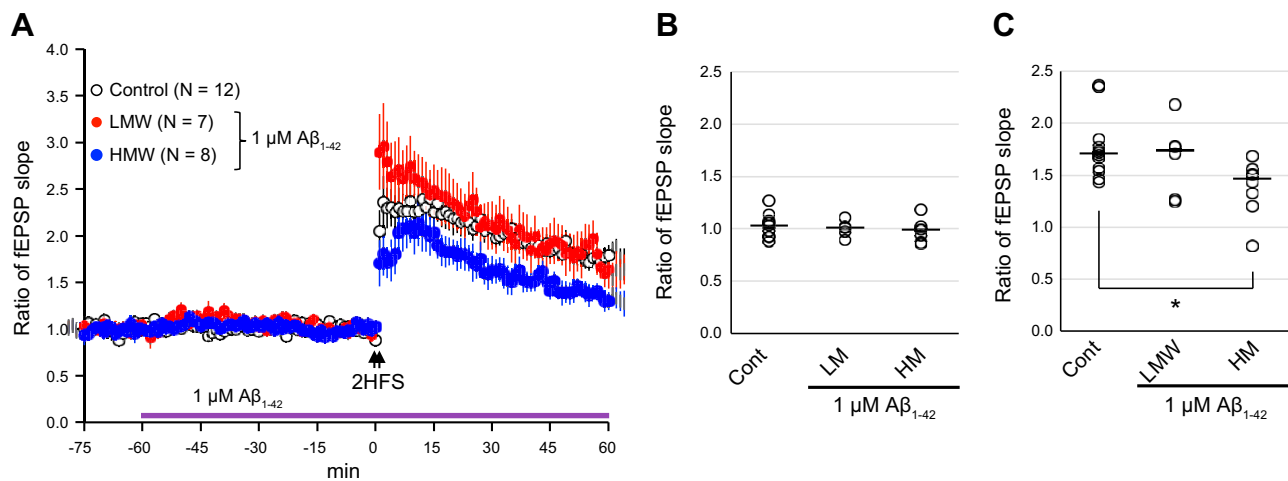
Figure 7. HMW-Aβ$_{1-42}$ inhibits hippocampal LTP. *A*) Time course of fEPSP slope is indicated. The color markers with error bar indicate mean ± SEM of each experimental group as follows: white: control, red: LMW-Aβ$_{1-42}$, and blue: HMW-Aβ$_{1-42}$. The 0 min point of the horizontal axis is the time of the first HFS train. Arrows indicate the 2 HFS trains. *B*) Basal fEPSP slopes of control and Aβ$_{1-42}$-treated hippocampal slices are indicated. In the treatment groups, fEPSP slopes were obtained after 50–60 min of Aβ$_{1-42}$ exposure. *C*) fEPSP slopes 50–60 min after HFS. Bars and scattered circles indicate medians and individual experimental values, respectively. *P < 0.05, control *vs.* HMW-Aβ$_{1-42}$ group.

potential and metabolic uncoupling. Although there are studies suggesting the disruption of membrane integrity by Aβ (38), definitive conclusions are hindered by the differences in experimental conditions and peptide preparation.

To elucidate the dominant mechanisms of Aβ oligomer–induced neuronal damage, including membrane damage, we studied the cellular responses to LMW and HMW-Aβ oligomer exposure using multiple indices of membrane integrity, cytolysis, oxidative stress, and synaptic function. We found that cell membrane and metabolic integrity were more severely disrupted by HMW-Aβ$_{1-42}$ than LMW-Aβ$_{1-42}$ as evidenced by the MTT cell viability assay, LDH leakage assay, calcein and ethidium homodimer-1 (live/dead) cell staining, WST assay, fluorometric measure of ROS generation and [Ca^{2+}]$_i$, lipid peroxidation assays, membrane fluidity measures, and electrophysiological recordings. Results of LDH and calcein and ethidium homodimer-1 assays that reflect cell membrane damage were clearly different between LMW-Aβ$_{1-42}$ and HMW-Aβ$_{1-42}$, but in the MTT and WST assays that reflect mitochondrial enzyme activity, the difference between both Aβs was not big. From these results, in short-term Aβ$_{1-42}$ treatment, Aβ$_{1-42}$ may first attack the cell membrane and subsequently induce damage to mitochondria. The degree of cell membrane damage was more severe in HMW-Aβ$_{1-42}$ than LMW-Aβ$_{1-42}$.

Many studies have reported that oxidative stress, which occurs in the presence of a physiologic imbalance between ROS generation and antioxidant capacity, is a critical pathogenic mechanism in AD progression (39). Indeed, in the brains of patients at different AD stages, increased oxidative stress marker levels are present (40). For example, the levels of lipid peroxide markers such as 4-hydroxyhexenal are constantly elevated during the early mild cognitive impairment and preclinical AD stages

compared with healthy control subjects and patients with late-stage AD (41). Along with the direct destruction/modification of lipids, DNA and proteins, the byproducts of lipid peroxidation produced during oxidative stress cause damage to the mitochondria and up-regulate tau phosphorylation, which appears essential for NFT formation (42). Because the redox properties of these different Aβ conformations are complex, the mechanisms of ROS generation in AD are unclear. The contribution of Aβ to oxidative stress is suggested by its metal-binding capacity (particularly for Cu^{2+}) and its ability to reduce Cu^{2+} and Fe^{3+} to Cu$^+$ and Fe^{2+}, which can then catalyze the generation of highly reactive superoxide anions from H$_2$O$_2$ *via* the Fenton reaction (43). Indeed, Aβ-induced ROS generation has been repeatedly demonstrated using various detection methods (44, 45). Generation of superoxide by Aβ may lead to mitochondrial impairment and further ROS generation, thereby establishing a positive feedback pathway that ultimately results in cell death (46). Gunn *et al.* (8) reported that Cu^{2+}-oxidized small oligomers of Aβ$_{1-42}$ bind to neurons and cause loss of plasma membrane integrity through lipid peroxidation. Further, Aβ may directly interact with the mitochondrial respiratory chain, causing metabolic dysfunction and increased ROS production (47), which is consistent with the clinical observations related to mitochondrial oxidative damage with AD progression (39). Fluorescent dye studies using model membranes have reported that aggregated Aβ damages cells by reducing membrane fluidity (48, 49), whereas it was recently reported that small Aβ oligomers had the opposite effect by reducing membrane cholesterol content (50). In the current study, we report that HMW-Aβ$_{1-42}$ reduces the fluidity of neuronal membranes to a significantly greater extent than LMW-Aβ$_{1-42}$. Thus, it is possible that the influence on membrane fluidity and ensuing neuronal damage depends on the specific Aβ conformation.

The effect of LMW-Aβ$_{1-42}$ and HMW-Aβ$_{1-42}$ was not different in the peaks immediately after exposure, however, at subsequent sustained plateau levels of [Ca^{2+}]$_i$, HMW-Aβ$_{1-42}$ exposure maintained higher levels than those induced by LMW-Aβ$_{1-42}$. On the other hand, we observed reduced depolarization-induced [Ca^{2+}]$_i$ influx through voltage-dependent Ca^{2+} channels following longer HMW-Aβ$_{1-42}$ treatment. These results suggested that HMW-Aβ$_{1-42}$ may not only damage voltage-gated calcium channels directly for a short time but also alter the cell membrane environment required for proper channel insertion or gating for a long time as evidenced by lipid peroxidation and membrane fluidity measurements.

Pretreatment with nicardipine significantly decreased the HMW-Aβ$_{1-42}$-induced increase in [Ca^{2+}]$_i$, suggesting that HMW-Aβ$_{1-42}$ promotes calcium influx through L-type VDCCs and that cells are not able to appropriately buffer the increase. Furthermore, pretreatment with nicardipine plus memantine resulted in a marked reduction of [Ca^{2+}]$_i$ compared to pretreatment with nicardipine alone. These findings suggest that both Aβs promotes calcium influx through L-type VDCC and NMDA receptors in SH-SY5Y cells. However, nicardipine plus memantine did not completely suppress the Aβ$_{1-42}$-induced [Ca^{2+}]$_i$ increase, suggesting activation of other influx or release pathways. It is reported, for example, that Aβ$_{1-42}$ oligomer may activate the α-amino-3-hydroxy-5-methyl-4-isoxazolepropionic acid receptor and store-operated calcium channel (14). Furthermore, NMDA receptor activity could be promoted by Aβ$_{1-42}$-evoked depolarization. A sustained increase in [Ca^{2+}]$_i$ by Aβ$_{1-42}$ may also cause mitochondrial Ca^{2+} overload, which in turn would promote the generation of ROS such as superoxide radicals. In addition, the release of apoptosis-inducing mitochondrial proteins including cytochrome c and increased [Ca^{2+}]$_i$ have been suggested to be the major effectors of neuronal cell death or neurodegeneration in several AD models (51).

Ca^{2+} homeostasis disruption is recognized as a potential mechanism related to AD neurodegeneration. It has been shown that elevated [Ca^{2+}]$_i$ results from both tau phosphorylation and mitochondrial damage, leading to further increases in ROS and [Ca^{2+}]$_i$ and finally to cell death (52). The increase in ROS generation and lipid peroxidation as well as the decrease in membrane fluidity induced by Aβ oligomers promote Ca^{2+} influx through VDCCs and NMDA receptors (14, 53). In addition, Aβ oligomers have been suggested to have the ability of penetrating and inserting into membranes, coating or lying on membrane surfaces, and potentially acting as cell-penetrating peptides (38). The detergent-like permeation of Aβ peptide into lipid membranes is suggested to occur by the association of amyloid-forming peptides in micelle-like structures. Further, membrane permeation takes place at high local peptide concentrations on the membrane surface after the covering of the surface with peptide monomers or oligomers or by an association between
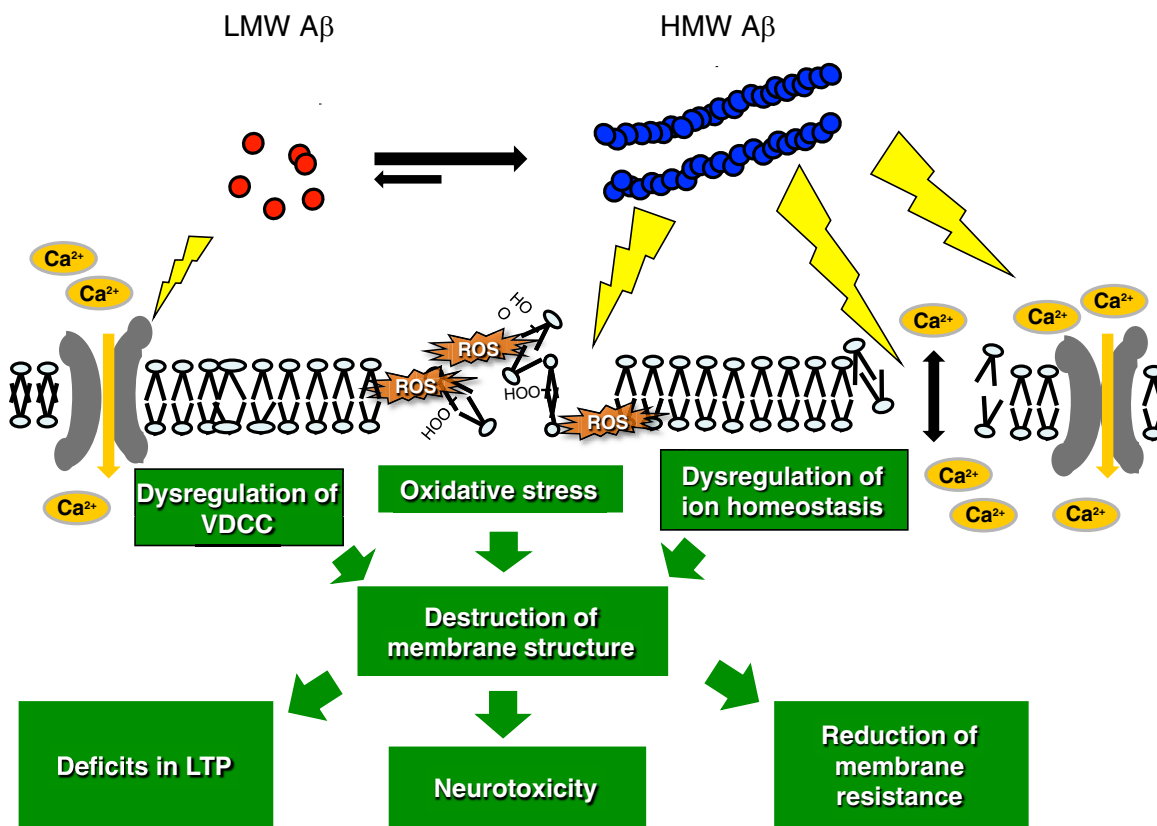

Figure 8. Schematic representation of Aβ neurotoxicity through membrane disruption. Although the various isoforms of aggregated Aβ are related to the pathogenesis of AD, oligomers such as HMW-Aβ$_{1-42}$ are more damaging to neuronal membranes than LMW-Aβ$_{1-42}$.

membrane-bound amyloid fibrils (54). It has been recently suggested that small oligomers of Aβ have higher affinity for HEK293T cell membranes than monomers (21), which is consistent with the greater cytotoxicity of HMW-Aβ$_{1-42}$ than LMW-Aβ$_{1-42}$. The initial interaction may be electrostatically driven, whereby Aβ preferentially binds to lipid headgroups or receptors on the membrane surface (55). Aβ can insert directly into lipid bilayers and form pores, a phenomenon first observed with artificial membranes (18). Similarly, Aβ$_{1-42}$ can assemble into a pore-forming β-barrel Aβ oligomeric structure, whereas Aβ$_{1-40}$ aggregates into amyloid fibrils under optimized detergent micelle conditions (20). Recently, it was reported that Aβ oligomers can irreversibly insert into the membrane and spontaneously form ion channels (19), and a recent simulation study indicated that membrane lipid peroxidation promotes this pore formation (56). Extracellular application of spherical Aβ$_{1-42}$ oligomers caused a large and rapid $[Ca^{2+}]_i$ elevation concomitant with increased membrane permeability in SH-SY5Y cells and oocytes (13, 57). Individual Aβ oligomers larger than trimers reportedly induced Ca^{2+} entry by crossing the plasma membrane rather than by acting on cellular receptors (58). Thus, the toxicity associated with Aβ oligomers may involve numerous distinct mechanisms, including effects on specific membrane proteins and general lipid damage, depending on conformation, concentration, cell type, and cell status. Nonetheless, disruption of biologic membranes appears to be a common pathogenic mechanism for different Aβ aggregation states.

Consistent with the changes in $[Ca^{2+}]_i$ and loss of membrane integrity, application of HMW-Aβ$_{1-42}$, but not LMW-Aβ$_{1-42}$, also depolarized SH-SY5Y cells and significantly reduced membrane input resistance. Bode *et al.* (59) monitored transmembrane currents during Aβ exposure to the extracellular face of the excised membranes from HEK293 cells and found that circular small Aβ$_{1-42}$ oligomers formed ion channels, whereas Aβ$_{1-40}$ oligomers, as well as fibrils and monomers, did not. Drolle *et al.* (60) used multicomponent lipid models with the aim to mimic healthy and AD states of neuronal membranes and posited that Aβ$_{1-42}$ increases lipid membrane roughness and increases membrane conductance, possibly through pore formation. Taken together, the $[Ca^{2+}]_i$ increase evoked by Aβ$_{1-42}$ oligomers may be due to pore formation and oxidative damage as well as suppression of calcium egress and sequestration pathways secondary to metabolic disruption.

Finally, we demonstrated that HMW-Aβ$_{1-42}$ significantly inhibited LTP formation in the mouse hippocampal CA1 subfield. Both LMW and HMW oligomers of Aβ have been reported to suppress LTP (5, 7), which may contribute to cognitive impairment that is observed in the early stages of AD before neurodegeneration (61). Excessive ROS accumulation reportedly inhibits LTP (62). In addition, membrane fluidity has been implicated in LTP and learning (63) and decreases in aged animals with learning and LTP deficits (64). These findings suggest that ROS generation and decreased membrane fluidity induced by HMW-Aβ impair the molecular, cellular, and synaptic properties essential for learning. Furthermore, membrane

pore formation may also impair cellular and synaptic functions (65, 66), and it is consistent with the observed loss of membrane integrity demonstrated by MTT, LDH, and calcein/ethidium homodimer-1 assays, $[Ca^{2+}]_i$ elevation, resting membrane potential increase, input resistance decrease, and LTP impairment. Taken together, our results demonstrated multiple mechanisms of Aβ oligomer–induced neuronal injury and death (**Fig. 8**).

Our findings suggest the possibility that reduction of HMW-Aβ$_{1-42}$ assemblies, such as PFs, may inhibit AD-associated neuronal damage by not only suppressing Aβ plaque accumulation but also reducing the direct membrane toxicity of HMW-Aβ$_{1-42}$.

AUTHOR CONTRIBUTIONS

M. Tsuji, H. Nishijo, and K. Ono designed research; T Yasumoto, Y. Takamura, M. Tsuji, T. Nakayama-Watanabe, K. Imamura, H. Inoue, S. Nakamura, A. Kimura, H. Nishijo, and K. Ono performed research; T. Yasumoto, Y. Takamura, M. Tsuji, T. Nakayama-Watanabe, K. Imamura, H. Inoue, S. Nakamura, T. Inoue, S. Yano, H. Nishijo, Y. Kiuchi, D. B. Teplow, and K. Ono wrote the manuscript.

REFERENCES

1. Selkoe, D. J., and Hardy, J. (2016) The amyloid hypothesis of Alzheimer's disease at 25 years. *EMBO Mol. Med.* **8**, 595–608
2. Hardy, J., and Selkoe, D. J. (2002) The amyloid hypothesis of Alzheimer's disease: progress and problems on the road to therapeutics. *Science* **297**, 353–356
3. Ono, K. (2018) Alzheimer's disease as oligomeropathy. *Neurochem. Int.* **119**, 57–70
4. Hartley, D. M., Walsh, D. M., Ye, C. P., Diehl, T., Vasquez, S., Vassilev, P. M., Teplow, D. B., and Selkoe, D. J. (1999) Protofibrillar intermediates of amyloid β-protein induce acute electrophysiological changes and progressive neurotoxicity in cortical neurons. *J. Neurosci.* **19**, 8876–8884
5. Walsh, D. M., Klyubin, I., Fadeeva, J. V., Cullen, W. K., Anwyl, R., Wolfe, M. S., Rowan, M. J., and Selkoe, D. J. (2002) Naturally secreted oligomers of amyloid β protein potently inhibit hippocampal long-term potentiation in vivo. *Nature* **416**, 535–539
6. Ono, K., Condron, M. M., and Teplow, D. B. (2009) Structure-neurotoxicity relationships of amyloid β-protein oligomers. *Proc. Natl. Acad. Sci. USA* **106**, 14745–14750
7. Ono, K., Li, L., Takamura, Y., Yoshiike, Y., Zhu, L., Han, F., Mao, X., Ikeda, T., Takasaki, J., Nishijo, H., Takashima, A., Teplow, D. B., Zagorski, M. G., and Yamada, M. (2012) Phenolic compounds prevent amyloid β-protein oligomerization and synaptic dysfunction by site-specific binding. *J. Biol. Chem.* **287**, 14631–14643

8. Gunn, A. P., Wong, B. X., Johanssen, T., Griffith, J. C., Masters, C. L., Bush, A. I., Barnham, K. J., Duce, J. A., and Cherny, R. A. (2016) Amyloid-β peptide Aβ3pE-42 induces lipid peroxidation, membrane permeabilization, and calcium influx in neurons. *J. Biol. Chem.* **291**, 6134–6145

9. Nussbaum, J. M., Schilling, S., Cynis, H., Silva, A., Swanson, E., Wangsanut, T., Tayler, K., Wiltgen, B., Hatami, A., Rönicke, R., Reymann, K., Hutter-Paier, B., Alexandru, A., Jagla, W., Graubner, S., Glabe, C. G., Demuth, H. U., and Bloom, G. S. (2012) Prion-like behaviour and tau-dependent cytotoxicity of pyroglutamylated amyloid-β. *Nature* **485**, 651–655

10. Nilsberth, C., Westlind-Danielsson, A., Eckman, C. B., Condron, M. M., Axelman, K., Forsell, C., Stenh, C., Luthman, J., Teplow, D. B., Younkin, S. G., Näslund, J., and Lannfelt, L. (2001) The 'Arctic' APP mutation (E693G) causes Alzheimer's disease by enhanced Abeta protofibril formation. *Nat. Neurosci.* **4**, 887–893

11. Lee, J., Gillman, A. L., Jang, H., Ramachandran, S., Kagan, B. L., Nussinov, R., and Teran Arce, F. (2014) Role of the fast kinetics of pyroglutamate-modified amyloid-β oligomers in membrane binding and membrane permeability. *Biochemistry* **53**, 4704–4714

12. Ikeda, K., Yamaguchi, T., Fukunaga, S., Hoshino, M., and Matsuzaki, K. (2011) Mechanism of amyloid β-protein aggregation mediated by GM1 ganglioside clusters. *Biochemistry* **50**, 6433–6440

13. Demuro, A., Smith, M., and Parker, I. (2011) Single-channel Ca(2+) imaging implicates Aβ1-42 amyloid pores in Alzheimer's disease pathology. *J. Cell Biol.* **195**, 515–524

14. Tan, Y., Deng, Y., and Qing, H. (2012) Calcium channel blockers and Alzheimer's disease. *Neural Regen. Res.* **7**, 137–140

15. Butterfield, D. A., Drake, J., Pocernich, C., and Castegna, A. (2001) Evidence of oxidative damage in Alzheimer's disease brain: central role for amyloid β-peptide. *Trends Mol. Med.* **7**, 548–554

16. Mattson, M. P., Cheng, B., Davis, D., Bryant, K., Lieberburg, I., and Rydel, R. E. (1992) β-Amyloid peptides destabilize calcium homeostasis and render human cortical neurons vulnerable to excitotoxicity. *J. Neurosci.* **12**, 376–389

17. Smale, G., Nichols, N. R., Brady, D. R., Finch, C. E., and Horton, W. E., Jr. (1995) Evidence for apoptotic cell death in Alzheimer's disease. *Exp. Neurol.* **133**, 225–230

18. Arispe, N. (2004) Architecture of the Alzheimer's A β P ion channel pore. *J. Membr. Biol.* **197**, 33–48

19. Jang, H., Connelly, L., Arce, F. T., Ramachandran, S., Kagan, B. L., Lal, R., and Nussinov, R. (2013) Mechanisms for the insertion of toxic, fibril-like β-amyloid oligomers into the membrane. *J. Chem. Theory Comput.* **9**, 822–833

20. Serra-Batiste, M., Ninot-Pedrosa, M., Bayoumi, M., Gairí, M., Maglia, G., and Carulla, N. (2016) Aβ42 assembles into specific β-barrel pore-forming oligomers in membrane-mimicking environments. *Proc. Natl. Acad. Sci. USA* **113**, 10866–10871

21. Sarkar, B., Das, A. K., and Maiti, S. (2013) Thermodynamically stable amyloid-β monomers have much lower membrane affinity than the small oligomers. *Front. Physiol.* **4**, 84

22. Bitan, G., Kirkitadze, M. D., Lomakin, A., Vollers, S. S., Benedek, G. B., and Teplow, D. B. (2003) Amyloid beta -protein (Abeta) assembly: abeta 40 and Abeta 42 oligomerize through distinct pathways. *Proc. Natl. Acad. Sci. USA* **100**, 330–335

23. Watanabe-Nakayama, T., Ono, K., Itami, M., Takahashi, R., Teplow, D. B., and Yamada, M. (2016) High-speed atomic force microscopy reveals structural dynamics of amyloid β1-42 aggregates. *Proc. Natl. Acad. Sci. USA* **113**, 5835–5840

24. Walsh, D. M., Hartley, D. M., Kusumoto, Y., Fezoui, Y., Condron, M. M., Lomakin, A., Benedek, G. B., Selkoe, D. J., and Teplow, D. B. (1999) Amyloid beta-protein fibrillogenesis. Structure and biological activity of protofibrillar intermediates. *J. Biol. Chem.* **274**, 25945–25952

25. Ando, T., Kodera, N., Takai, E., Maruyama, D., Saito, K., and Toda, A. (2001) A high-speed atomic force microscope for studying biological macromolecules. *Proc. Natl. Acad. Sci. USA* **98**, 12468–12472

26. Uchihashi, T., Kodera, N., and Ando, T. (2012) Guide to video recording of structure dynamics and dynamic processes of proteins by high-speed atomic force microscopy. *Nat. Protoc.* **7**, 1193–1206

27. Watanabe-Nakayama, T., and Ono, K. (2018) High-speed atomic force microscopy of individual amyloidogenic protein assemblies. *Methods Mol. Biol.* **1814**, 201–212

28. Krishtal, J., Bragina, O., Metsla, K., Palumaa, P., and Tõugu, V. (2017) In situ fibrillizing amyloid-β 1-42 induces neurite degeneration and apoptosis of differentiated SH-SY5Y cells. *PLoS One* **12**, e0186636

29. Nakagawa, M., Taniguchi, Y., Senda, S., Takizawa, N., Ichisaka, T., Asano, K., Morizane, A., Doi, D., Takahashi, J., Nishizawa, M., Yoshida, Y., Toyoda, T., Osafune, K., Sekiguchi, K., and Yamanaka, S. (2014) A novel efficient feeder-free culture system for the derivation of human induced pluripotent stem cells. *Sci. Rep.* **4**, 3594

30. Imamura, K., Sahara, N., Kanaan, N. M., Tsukita, K., Kondo, T., Kutoku, Y., Ohsawa, Y., Sunada, Y., Kawakami, K., Hotta, A., Yawata, S., Watanabe, D., Hasegawa, M., Trojanowski, J. Q., Lee, V. M., Suhara, T., Higuchi, M., and Inoue, H. (2016) Calcium dysregulation contributes to neurodegeneration in FTLD patient iPSC-derived neurons. *Sci. Rep.* **6**, 34904

31. Okimotoa, Y., Watanabea, A., Nikia, E., Yamashitab, T., and Noguchia, N. (2000) A novel fluorescent probe diphenyl-1-pyrenylphosphine to follow lipid peroxidation in cell membranes. *FEBS Lett.* **474**, 137–140

32. Walsh, D. M., Lomakin, A., Benedek, G. B., Condron, M. M., and Teplow, D. B. (1997) Amyloid beta-protein fibrillogenesis. Detection of a protofibrillar intermediate. *J. Biol. Chem.* **272**, 22364–22372

33. Ono, K., Condron, M. M., and Teplow, D. B. (2010) Effects of the English (H6R) and Tottori (D7N) familial Alzheimer disease mutations on amyloid β-protein assembly and toxicity. *J. Biol. Chem.* **285**, 23186–23197

34. Irvine, G. B., El-Agnaf, O. M., Shankar, G. M., and Walsh, D. M. (2008) Protein aggregation in the brain: the molecular basis for Alzheimer's and Parkinson's diseases. *Mol. Med.* **14**, 451–464

35. Savage, M. J., Kalinina, J., Wolfe, A., Tugusheva, K., Korn, R., Cash-Mason, T., Maxwell, J. W., Hatcher, N. G., Haugabook, S. J., Wu, G., Howell, B. J., Renger, J. J., Shughrue, P. J., and McCampbell, A. (2014) A sensitive aβ oligomer assay discriminates Alzheimer's and aged control cerebrospinal fluid. *J. Neurosci.* **34**, 2884–2897

36. Xia, W., Yang, T., Shankar, G., Smith, I. M., Shen, Y., Walsh, D. M., and Selkoe, D. J. (2009) A specific enzyme-linked immunosorbent assay for measuring β-amyloid protein oligomers in human plasma and brain tissue of patients with Alzheimer disease. *Arch. Neurol.* **66**, 190–199

37. Takeda, S., Hashimoto, T., Roe, A. D., Hori, Y., Spires-Jones, T. L., and Hyman, B. T. (2013) Brain interstitial oligomeric amyloid β increases with age and is resistant to clearance from brain in a mouse model of Alzheimer's disease. *FASEB J.* **27**, 3239–3248

38. Williams, T. L., and Serpell, L. C. (2011) Membrane and surface interactions of Alzheimer's Aβ peptide–insights into the mechanism of cytotoxicity. *FEBS J.* **278**, 3905–3917

39. Rosini, M., Simoni, E., Milelli, A., Minarini, A., and Melchiorre, C. (2014) Oxidative stress in Alzheimer's disease: are we connecting the dots? *J. Med. Chem.* **57**, 2821–2831

40. Hilt, S., Altman, R., Kálai, T., Maezawa, I., Gong, Q., Wachsmann-Hogiu, S., Jin, L. W., and Voss, J. C. (2018) A bifunctional anti-amyloid blocks oxidative stress and the accumulation of intraneuronal amyloid-beta. *Molecules* **23**, E2010

41. Bradley, M. A., Xiong-Fister, S., Markesbery, W. R., and Lovell, M. A. (2012) Elevated 4-hydroxyhexenal in Alzheimer's disease (AD) progression. *Neurobiol. Aging* **33**, 1034–1044

42. Ansari, M. A., and Scheff, S. W. (2010) Oxidative stress in the progression of Alzheimer disease in the frontal cortex. *J. Neuropathol. Exp. Neurol.* **69**, 155–167

43. Cheignon, C., Tomas, M., Bonnefont-Rousselot, D., Faller, P., Hureau, C., and Collin, F. (2018) Oxidative stress and the amyloid β peptide in Alzheimer's disease. *Redox Biol.* **14**, 450–464

44. Smith, D. G., Cappai, R., and Barnham, K. J. (2007) The redox chemistry of the Alzheimer's disease amyloid β peptide. *Biochim. Biophys. Acta* **1768**, 1976–1990

45. Hureau, C., and Faller, P. (2009) Abeta-mediated ROS production by Cu ions: structural insights, mechanisms and relevance to Alzheimer's disease. *Biochimie* **91**, 1212–1217

46. Pohanka, M. (2014) Alzheimer´s disease and oxidative stress: a review. *Curr. Med. Chem.* **21**, 356–364

47. Hernandez-Zimbron, L. F., Luna-Muñoz, J., Mena, R., Vazquez-Ramirez, R., Kubli-Garfias, C., Cribbs, D. H., Manoutcharian, K., and Gevorkian, G. (2012) Amyloid-β peptide binds to cytochrome C oxidase subunit 1. *PLoS One* **7**, e42344

48. Kremer, J. J., Pallitto, M. M., Sklansky, D. J., and Murphy, R. M. (2000) Correlation of β-amyloid aggregate size and hydrophobicity with decreased bilayer fluidity of model membranes. *Biochemistry* **39**, 10309–10318

49. Yip, C. M., Darabie, A. A., and McLaurin, J. (2002) Abeta42-peptide assembly on lipid bilayers. *J. Mol. Biol.* **318**, 97–107

50. Fernández-Pérez, E. J., Sepúlveda, F. J., Peters, C., Bascuñán, D., Riffo-Lepe, N. O., González-Sanmiguel, J., Sánchez, S. A., Peoples, R. W., Vicente, B., and Aguayo, L. G. (2018) Effect of cholesterol on

membrane fluidity and association of Aβ oligomers and subsequent neuronal damage: a double-edged sword. *Front. Aging Neurosci.* **10**, 226

51. Stutzmann, G. E. (2007) The pathogenesis of Alzheimers disease is it a lifelong "calciumopathy"? *Neuroscientist* **13**, 546–559

52. Supnet, C., and Bezprozvanny, I. (2010) The dysregulation of intracellular calcium in Alzheimer disease. *Cell Calcium* **47**, 183–189

53. Zhu, D., Bungart, B. L., Yang, X., Zhumadilov, Z., Lee, J. C., and Askarova, S. (2015) Role of membrane biophysics in Alzheimer's-related cell pathways. *Front. Neurosci.* **9**, 186

54. Shai, Y. (1999) Mechanism of the binding, insertion and destabilization of phospholipid bilayer membranes by α-helical antimicrobial and cell non-selective membrane-lytic peptides. *Biochim. Biophys. Acta* **1462**, 55–70

55. Tofoleanu, F., and Buchete, N. V. (2012) Molecular interactions of Alzheimer's Aβ protofilaments with lipid membranes. *J. Mol. Biol.* **421**, 572–586

56. Van der Paal, J., Neyts, E. C., Verlackt, C. C. W., and Bogaerts, A. (2016) Effect of lipid peroxidation on membrane permeability of cancer and normal cells subjected to oxidative stress. *Chem. Sci. (Camb.)* **7**, 489–498

57. Demuro, A., Mina, E., Kayed, R., Milton, S. C., Parker, I., and Glabe, C. G. (2005) Calcium dysregulation and membrane disruption as a ubiquitous neurotoxic mechanism of soluble amyloid oligomers. *J. Biol. Chem.* **280**, 17294–17300

58. Drews, A., Flint, J., Shivji, N., Jönsson, P., Wirthensohn, D., De Genst, E., Vincke, C., Muyldermans, S., Dobson, C., and Klenerman, D. (2016) Individual aggregates of amyloid β induce temporary calcium influx through the cell membrane of neuronal cells. *Sci. Rep.* **6**, 31910

59. Bode, D. C., Baker, M. D., and Viles, J. H. (2017) Ion channel formation by amyloid-β42 oligomers but not amyloid-β40 in cellular membranes. *J. Biol. Chem.* **292**, 1404–1413

60. Drolle, E., Negoda, A., Hammond, K., Pavlov, E., and Leonenko, Z. (2017) Changes in lipid membranes may trigger amyloid toxicity in Alzheimer's disease. *PLoS One* **12**, e0182194

61. Rowan, M. J., Klyubin, I., Cullen, W. K., and Anwyl, R. (2003) Synaptic plasticity in animal models of early Alzheimer's disease. *Philos. Trans. R. Soc. Lond. B Biol. Sci.* **358**, 821–828

62. Massaad, C. A., and Klann, E. (2011) Reactive oxygen species in the regulation of synaptic plasticity and memory. *Antioxid. Redox Signal.* **14**, 2013–2054

63. Schaeffer, E. L., Bassi, F., Jr., and Gattaz, W. F. (2005) Inhibition of phospholipase A2 activity reduces membrane fluidity in rat hippocampus. *J. Neural Transm. (Vienna)* **112**, 641–647

64. Fukaya, T., Gondaira, T., Kashiyae, Y., Kotani, S., Ishikura, Y., Fujikawa, S., Kiso, Y., and Sakakibara, M. (2007) Arachidonic acid preserves hippocampal neuron membrane fluidity in senescent rats. *Neurobiol. Aging* **28**, 1179–1186

65. Alzheimer's Association Calcium Hypothesis Workgroup. (2017) Calcium hypothesis of Alzheimer's disease and brain aging: a framework for integrating new evidence into a comprehensive theory of pathogenesis. *Alzheimers Dement* **13**, 178–182.e17

66. Berridge, M. J. (2017) Calcium signalling in health and disease. *Biochem. Biophys. Res. Commun.* **485**, 5